# Multidecadal climate variability over northern France during the past 500 years and its relation to large-scale atmospheric circulation

Dieppois, B, Lawler, D, Slonosky, V, Massei, N, Bigot, S, Fournier, M & Durand, A



**Original citation & hyperlink:**
Dieppois, B, Lawler, D, Slonosky, V, Massei, N, Bigot, S, Fournier, M & Durand, A 2016, 'Multidecadal climate variability over northern France during the past 500 years and its relation to large-scale atmospheric circulation' *International Journal of Climatology*, vol 36, no. 15, pp. 4679-4696
https://dx.doi.org/10.1002/joc.4660

DOI 10.1002/joc.4660
ISSN 0899-8418
ESSN 1097-0088

Publisher: Wiley

INTERNATIONAL JOURNAL OF CLIMATOLOGY

# Multidecadal climate variability over northern France during the past 500 years and its relation to large-scale atmospheric circulation



| | |
|---|---|
| Journal: | *International Journal of Climatology* |
| Manuscript ID | JOC-15-0171.R1 |
| Wiley - Manuscript type: | Research Article |
| Date Submitted by the Author: | 09-Oct-2015 |



| | |
|---|---|
| Complete List of Authors: | Dieppois, Bastien; University of Cape Town, African Climate Development and Initiative<br>Lawler, Damian; Coventry University, Centre for Agroecology, Water and Resilience (CAWR)<br>Slonosky, Victoria; anadian Historical Climate Data Project, Data Analysis<br>Massei, N; UMR 6143 M2C, University of Rouen, Department of Geology;<br>Bigot, Sylvain; Université de Grenoble, Geography;<br>Fournier, Matthieu; UMR CNRS 6143 Morhodynamique Continentale et Côtière, Université de Rouen, FED 4116 SCALE, Geology<br>Durand, Alain; CNRS UMR 6143, Geology |



| | |
|---|---|
| Keywords: | Northern France, Precipitation, Climate, River flow changes, Multidecadal variability, North Atlantic Oscillation, Atmospheric circulation, Non-stationarity |

# Multidecadal climate variability over northern France during the past 500 years and its relation to large-scale atmospheric circulation

Dieppois B.[1, 2], Lawler D.M. [1], Slonosky V.[3], Massei N.[2], Bigot S. [4], Fournier M.[2], Durand A.[2]
bastien.dieppois@univ-rouen.fr

[1] Centre for Agroecology, Water and Resilience (CAWR), Coventry University, Coventry CV1 5FB, United Kingdom
[2] Laboratoire Morphodynamique Continentale et Côtière (M2C), Université de Rouen, CNRS UMR 6143, FED 4116 SCALE, Mont-Saint Aignan, France
[3] Canadian Historical Data Rescue, Montreal, Canada
[4] Laboratoire d'étude des Transferts en Hydrologie et Environnement (LTHE), Université Grenoble Alpes (UGA), Grenoble, France

**Running title:** Multidecadal climate variability over northern France

**Abstract:** We examine secular changes and multidecadal climate variability on a seasonal scale in northern France over the last 500 years, and examine the extent to which they are driven by large-scale atmospheric variability. Multiscale trend analysis and segmentation procedures show statistically significant increases of winter and spring precipitation amounts in Paris since the end of the 19th century. This changes the seasonal precipitation distribution from one with a pronounced summer peak at the end of the Little Ice Age to an almost uniform distribution in the 20th century. This switch is linked to an early warming trend in winter temperature. Changes in spring precipitation are also correlated with winter precipitation for time-scales greater than 50 years, which suggests a seasonal persistence. Hydrological modelling results show similar rising trends in river flow for the Seine at Paris. However, such secular trends in the seasonal climatic conditions over northern France are substantially modulated by irregular multidecadal (50–80 year) fluctuations. Furthermore, since the end of the 19th century, we find an increasing variance in multidecadal hydroclimatic winter and spring, and this coincides with an increase in the multidecadal North Atlantic Oscillation (NAO) variability, suggesting a significant influence of large-scale atmospheric circulation patterns. However, multidecadal NAO variability has decreased in summer. Using Empirical Orthogonal Function analysis, we detect multidecadal North Atlantic sea-level pressure anomalies, which are significantly linked to the NAO during the Modern period. In particular, a south-eastward (south-westward) shift of the Icelandic Low (Azores High) drives substantial multidecadal changes in spring. Wetter springs are likely to be driven by potential changes in moisture advection from the Atlantic, in response to northward shifts of North Atlantic storm tracks over European regions, linked to periods of positive NAO. Similar, but smaller, changes in rainfall are observed in winter.

**Keywords:** Northern France, Precipitation, Climate, River flow changes, Multidecadal variability, North Atlantic Oscillation, Atmospheric circulation, Non-stationarity

## 1. Introduction

While anthropogenic influence may contribute to recent and future temperature and precipitation trends, climate changes prior to the Industrial Revolution in the 18$^{th}$ century can be attributed to natural causes such as changes in solar activity, volcanic eruptions and natural changes in greenhouse gas concentration (*e.g.,* Jansen *et al*., 2007). In this context, knowledge concerning the range of variability in hydroclimatic variables such as seasonal precipitation, drought and river flow in past centuries at regional scales is important (*e.g.,* Lawler, 1987; Slonosky, 2002; Xoplaki *et al*., 2005; Pauling *et al*., 2006). Furthermore, linking such changes to large-scale atmospheric and oceanic oscillations is crucial to building an understanding of their controls.

European climate is known to be strongly related to the state of the atmospheric circulation over the North Atlantic (*e.g.,* Hurrell, 1995; Slonosky *et al*., 2001; Cassou *et al.*, 2004; Xoplaki *et al.*, 2005; Hurrell and Deser, 2009; Küttel *et al*., 2010). More specifically, the North Atlantic Oscillation (NAO) is described as a key driver of climate conditions over

Europe (Hurrell, 1995; Cassou *et al*., 2004; Hurrell and Deser, 2009), and is likely to influence hydrological systems (Philips *et al*., 2003; Kingston *et al*., 2006a, b, 2009; Massei *et al*., 2007; Lavers *et al*., 2010; Holman *et al*., 2011). The NAO can be described as an oscillation of atmospheric mass between the northern North Atlantic and the subtropical Atlantic, usually defined through changes in surface pressure (Hurrell, 1995; Cassou *et al.*, 2004; Hurrell and Deser, 2009). This oscillation, which is the only teleconnection pattern evident throughout the year in the northern Hemisphere (Barnston and Livezey, 1987; Hurrell *et al*., 2003), produces changes in wind speed and direction affecting heat and moisture transport between the Atlantic and the neighbouring European continent (Hurrell, 1995; Cassou *et al.*, 2004; Hurrell and Deser, 2009).

However, the links between NAO pattern and European hydroclimate are complex and poorly understood. In particular, the relationship are not constant over time, and show seasonal as well as long-term temporal nonstationarity (Slonosky and Yiou, 2002; Raible *et al*., 2006; Gamiz-Fortis *et al*., 2008; Fritier *et al*., 2012; Lehner *et al*., 2012). For instance, while positive winter NAO drives wetter conditions over northwestern Europe (Hurrell, 1995), positive summer NAO, which is displaced significantly north-eastward compared to winter, implies dryer conditions (Hurrell and Deser, 2009; Folland *et al.*, 2009). Similar changes in the position of the poles of the NAO also occur over longer time-scales, but the reasons are less well understood. According to Raible *et al.* (2014), who examined several control and transient millennium-scale simulations with coupled models, shifts in the centres of action of the NAO are not related to changes in external forcing. This is consistent with internal climate variability, such as North Atlantic sea-ice-atmosphere interactions (Hilmer and Jung, 2000; Jung *et al*., 2003). However, this contradicts other studies suggesting shifts in the NAO pattern under greenhouse-gas-induced warming (Ulbrich and Christoph, 1999; Dong *et al*., 2011), or in response to fluctuations in solar activity (Ineson *et al*., 2011; van Loon *et al*., 2012).

In particular, European climate between the 16th and 19th centuries has seen cold multi-decadal periods, within the period known as the "Little Ice Age" (LIA; Grove, 1988; Bradley and Jones, 1993; Jones *et al*., 1998; Luterbacher et al., 2004; Büntgen and Hellman, 2014). The most popular hypothesis of LIA climate change is a weakening of the Atlantic Meridional Overturning Circulation (AMOC) in response to a pervasive negative NAO, which implies both dry and cold anomalies over the northern regions of Europe (Luterbacher *et al*., 1999; Trouet *et al*., 2009; Mann *et al*., 2009; Trouet *et al*., 2012). However, contradictory evidence from other proxy-based studies suggests that the LIA was characterized by enhanced storminess over the northern North Atlantic (Meeker and Mayeki, 2002; Dawson *et al*., 2003, 2007), which is usually consistent with a positive NAO. Such multidecadal fluctuations in the NAO have also been reported over the last two centuries, hereafter referred to as the Modern period (Cook *et al*., 1998; Goodkin *et al*., 2008; Olsen *et al*., 2012; Dieppois *et al*., 2013; Sun *et al*., 2015), and in precipitation amounts in northern France (Dieppois *et al*., 2013) as well as French river flow (Boé and Habets, 2014). Analysing the annual relationship between NAO and precipitation in England and northern France back to the pre-industrial period, Dieppois *et al.* (2013) show a phase change at the multidecadal time-scale between the LIA and the Modern period: before 1850, negative NAO was associated with greater precipitation but, after 1850, positive NAO was associated with greater precipitation. This non-stationarity in the annual relationship might result from long-term changes in seasonal NAO patterns, but these have not yet been explored. This issue is especially problematic since multidecadal fluctuations in European and northern France hydroclimate, and in particular river flows, may also have serious impacts for society in influencing recent and future trends of water resources.

In this paper, using long-term climatic observations, reconstructions and conceptual hydrologic modelling back to 1500, we examine: i) how the annual cycles of hydroclimatic variables (precipitation, temperature, potential evapotranspiration [PE]) affecting northern France have changed since the end of the LIA; ii) how the multidecadal changes in the relationship between NAO and precipitation over northern France are related to changes in the seasonal relationship; iii) how river flow is affected by such changes, by examining streamflow of one of the main French rivers, the Seine River flow; iv) how North Atlantic Sea-Level Pressure (SLP) anomalies affected the multidecadal variability of the NAO after 1850.

The paper is organised as follows. In Section 2, we discuss the datasets used in this study, before we describe the analysis methods in Section 3. Seasonal changes and trends in hydroclimatic variables over the past 500 years are examined in Section 4.1. In Section 4.2, we investigate coherent seasonal changes in the multidecadal variability of northern France hydroclimate and of the NAO. Potential effects of such changes on Seine river flow are estimated by hydrological modelling in Section 4.3. The multidecadal North Atlantic SLP anomalies are then extracted for each season in Section 5.1, before describing their potential impacts on European precipitation during the Modern period (1820–2000, hereafter) in Section 5.2. Our main results are interpreted and their wider implications discussed in Section 6.

## 2. Data

### 2.1. Precipitation data

All datasets used in this paper are summarised schematically in Figure 1, together with their corresponding timescales. The Paris observations of monthly precipitation totals used for the study originate from updates to Slonosky (2002). They come from two main sources: the yearly summaries of the weather which were published in the *Mémoires de l'Academie Royale des Sciences* from 1688 to 1754, and previously published data collected by Emilien Renou (1815–1902) from 1806 to 1902 (Renou, 1885). Such time series can be affected by modifications of measurement conditions such as rain gauge displacements, especially height and exposure, measurement instrument replacement, or changes in rain gauge environment, which could result in artificial shifts that do not reflect climate variations. However, as suggested by Slonosky (2002) and Dieppois *et al.* (2013), this time series, once adjusted (*e.g.,* Tabony 1980, 1981), can be considered homogeneous. The spatial coherence of interannual Paris precipitation anomalies with larger scale precipitation fields between 1901 and 2009 has nevertheless been estimated empirically for each season in Figure 2 (*i.e.*, winter: DJF; spring: MAM; summer: JJA; autumn: SON). This is based on a pointwise correlation with high-resolution grids from the CRU TS 3.10.1 monthly datasets (explained at badc.nerc.ac.uk/view; Fig.1). The year-to-year variations of seasonal Paris precipitation series are significantly correlated with a large area of precipitation observations from the CRU data set over NW Europe with a maximum centred on Paris (Fig. 2a-d), suggesting robust spatial coherence of the data in all four seasons.

We also use the high-resolution precipitation reconstruction of Pauling *et al.* (2006) which covers the European land areas (30°N – 70°N; 30°W – 40°E) resolved on a 0.5°×0.5° grid (Fig.1). This reconstruction is based on transfer functions derived from Empirical Orthogonal Function (EOF) regression between predictors, such as long instrumental precipitation series or natural proxies, and the predictand (CRU TS 3.10 dataset). We established a northern France precipitation index from this reconstructed field using an average over latitudes 47.5°N – 50.5°N and longitudes 0 – 4°E. By comparing the reconstructed precipitation to the Paris observations with seasonal correlation maps, the reconstructed northern France precipitation index emerges as a useful, spatially coherent, representation of year-to-year fluctuations of northwestern European precipitation for all seasons (Fig. 2e-h).

Note that precipitation measurements from the Paris Observatory were used as predictor in the Pauling reconstruction (Pauling *et al*., 2006) and, thus, are not independent observations. However, in the present study, the observed Paris precipitation and the reconstructed northern France index is treated independently to avoid any circular argument.

**2.2. Temperature and Potential Evapotranspiration data**

The homogenized Central England Temperature index, which is the longest instrumental record of temperature in the world, has been used to examine temperature fluctuations that may have influenced the climate of northern France over the past five centuries (Fig.1). This monthly time-series, covering 1659 to 1973, was compiled by Manley (1974), before being updated by Parker *et al.* (1992). Although this index is representative of a roughly triangular area of the United Kingdom enclosed by Lancashire, London and Bristol, its interdecadal to multidecadal variability is almost identical to that of Paris temperature records (1757 – present; Fig.1), and the trend of the same order (Dieppois *et al*., 2013). Their seasonal correlations are between 0.7 and 0.82 at $p \leq 2.2^{e\text{-}16}$, with maximum and minimum in winter and autumn, respectively. We note differences in the mean, especially between spring and autumn (Paris T°C minus CET = 0.36°C in winter, -1.90°C in spring , -2.71°C in summer, -

1.24°C in autumn). Very similar results were, however, obtained using Paris temperature time series (as discussed hereafter).

We also calculated the potential evapotranspiration (PE, in mm), which forms a key part of catchment water budgets (Fig.1). PE is defined as the amount of evaporation and transpiration that would occur if sufficient water sources were available, *i.e.,* when soil moisture is not a limiting factor. The complexity of these calculations varies greatly, ranging from a simple function of just one atmospheric variable, often temperature (Thornthwaite, 1948), to those requiring a range of variables, such as relative humidity, wind speed and net solar radiation (*e.g.*, Hargreaves, 1994; Droogers and Allen, 2002). The *Thornthwaite* equation, which can be used when only temperature data are available, has been selected, and is given by:

$$\mathrm{PE} = 16\mathrm{N_m}\left(\frac{10\overline{\mathrm{T}}_\mathrm{m}}{\mathrm{I}}\right)^{\mathrm{a}}\ \mathrm{mm} \tag{1}$$

where m is the index for months with m = 1, 2, 3…12, $N_m$ is the monthly adjustment factor related to hours of daylight, $\overline{T}_m$ is the monthly mean air temperature (C), the exponent *a*, and *I* is the heat index for the year, given by :

$$\mathrm{I} = \sum \mathrm{i_m} = \sum\left(\frac{\overline{\mathrm{T}}_\mathrm{m}}{5}\right)^{1.5} \tag{2}$$

$$a = 6.7 \times 10^{-7} \times I^3 - 7.7 \times 10^{-5} \times I^2 + 1.8 \times 10^{-2} \times I + 0.49 \tag{3}$$

Estimates of PE were very similar using Central England or Paris temperatures (*Corr.[R]* ≥ 0.7; -11.6 mm ≤ *Mean Error [ME]* ≤ 2.3 mm; the ratio of Standard Devations [*rSD*] ≥ 0.66). Note, however, that such a simplified model of PE may respond with less accuracy to a warming climate than calculations based on the underlying physical principles, which take into changes relative humidity, wind speed and net solar radiation (Sheffield *et al.*, 2012).

### 2.3. Sea-Level Pressure data

In the atmospheric circulation analysis, we compare two observed and two reconstructed SLP fields over the North-Atlantic-European area (30°N – 70°N; 30°W – 40°E; Fig.1). The HadSLP2r dataset compiled by the Met Office Hadley Centre, which is resolved on a 5°×5° grid between 1850 and 2013, has been used as a reference over the instrumental period (Fig. 1; Allan and Ansell, 2006). We also used an extended observation field from the Annual to Decadal Variability In Climate in Europe (ADVICE) project (Fig. 1), which is based on a compilation and homogenization of 51 European stations with starting dates ranging from 1755 to 1871 (Jones *et al*., 1999). We used reconstructions performed by Luterbacher *et al.* (2002) and Küttel *et al.* (2010), which are both resolved on a 5°×5° grid but cover different periods (Fig. 1). These two reconstructions were computed by means of an EOF regression technique with predictors comprising early instrumental time series as well as several climate indices based on documentary proxy data from various sites in Europe. However, the reconstruction from Küttel *et al.* (2010), which only uses terrestrial instrumental pressure series and maritime wind information derived from ship logbook data, is more reliable over the eastern North Atlantic than the other early-instrumental SLP fields (Küttel *et al*., 2010). It should also be noted that precipitation (but not the Paris monthly observations) was used as predictor in the Luterbacher *et al*. (1999) reconstruction.

From these SLP datasets, the principal component (PC) time series of the leading EOF of reconstructed SLP anomalies over the Euro-Atlantic sector are calculated seasonally (*i.e.*, winter: DJF; spring: MAM; summer: JJA; autumn: SON) to define NAO indices. This ensures the ability to track the movement of the NAO centres of action through the annual cycle, and thus to provide an optimal representation of each seasonal NAO spatial pattern. Note that the varying start dates and lengths of the observed and reconstructed datasets lead to slightly different definitions of the Modern period (Fig. 1).

# 3. Methods

## 3.1. Estimation of seasonal and multidecadal variabilities

First, we examined the modifications of the seasonal temperature anomalies and of the seasonal precipitation distribution using a cartographic representation of observed and reconstructed values over centuries. Second, changes in the mean value of average seasonal temperature, PE, and precipitation were investigated using the segmentation procedure of Aksoy *et al.* (2008). This method uses a least squares algorithm to detect optimal breaks between adjacent data-segments with means that are significantly different using the *Scheffe* contrast test at $p = 0.05$. Third, monotonic trends in each seasonal average were calculated using a modified Mann-Kendall trend test accounting for serial correlation (Hamed and Rao, 1998). To eliminate the effect of serial correlation, the effective sample size, which allows us to modify the Mann-Kendall $S$ statistics, has been estimated according to a theoretical relationship based on first-order auto-regressive (AR[1]) model of the raw time series considered. In addition, to examine the influence of potential multidecadal fluctuations on trends (*i.e.*, the Sen's slope values; Sen, 1968), a rolling trend analysis across every possible time-scale has been used (Mc Cabe and Wolock, 2002; Liebman *et al*., 2010). The same approach has been employed to examine whether winter trends and variability in temperature and precipitation are statistically related to those of spring and summer months, and also if this is restricted to specific time-scales.

Potentially synchronous changes in precipitation, temperature, PE and NAO on multidecadal time-scales are then examined by submitting each seasonal time series to the Continuous Wavelet Transform (CWT). By representing the time series in the time-scale space, one can determine which scales of variability (or periods in a Fourier sense) are the dominant variability modes through time. It should be noted, however, that multi-proxy climate reconstructions using tree-ring proxies as predictors are likely to overestimate low-frequency signals (Franke *et al*., 2013). Such a decomposition of each seasonal signal is conducted with a Morlet mother wavelet with angular frequency 6 to produce the local wavelet spectra, which provides a good trade-off between time and frequency resolution. The detailed explanations of CWT methodology and its applications to the analysis of hydrological and climatic signals are now widely documented (*e.g.,* Torrence and Compo 1998; Maraun, 2006; Sang, 2013). The significance test of the wavelet spectrum for geophysical signals generally assumes a red noise background spectrum for the null hypothesis. The wavelet spectrum is tested for every point in time and scale to check whether the power exceeds a certain critical value determined by Monte-Carlo simulations of AR[1] processes. The cone of influence, which delineates the area under which power can be underestimated as a result of edge effects and zero padding, is also calculated and represented on all spectra as a thick bold line.

**3.2. Long-term Seine river flow reconstruction**

The potential effects of secular and multidecadal changes in precipitation, temperature and PE on the Seine River flow at Paris have been evaluated by hydrological modelling using GR2M (Génie Rural à 2 paramètres au pas de temps Mensuel; Mouelhi *et al*., 2006). GR2M is a two-store empirical lumped hydrological model running, which runs on a monthly time-step basis with two parameters: (a) the maximum capacity of the production store ($S$); and (b) the water exchange term with neighbouring catchments (*i.e.,* hydrographic network and aquifer) which applies to the routing store ($R$). The model is forced by monthly precipitation ($P$) and potential evapotranspiration ($PE$) and returns a monthly flow ($Q$). Note that the soil moisture storage capacity (parameters for store $S$) controls the response of the model to rain events, and to a certain extent, the variability of the simulated flow. As soil moisture storage capacity increases, the simulated flow depends less on the current rainfall and more on the storage level, itself dependent on past rainfall. To avoid any problems related to this issue our model initialization was defined according to Mouelhi *et al.* (2006). Note that very similar simulated river flow variability was obtained using Central England or Paris temperature ($R \geq 0.98$ and $rSD \geq 0.91$). However, using Central England temperature leads to underestimate simulated flow by a maximum of 22.64 $m^3.s^{-1}$ (~7.5%).

The simulated Paris river flow is then compared with the observed river flows from a gauging station in south-east Paris at Austerlitz, from 1885 to 2014. Metadata indicate that this river flow gauge is currently strongly influenced by human activity, but shows a good quality control (http://www.hydro.eaufrance.fr/). Artificial influence is principally related to reservoirs near the headwaters, built in 1973, which control up to 17% of river inputs. However, in our tests, we found no changes in homogeneity of the time series in 1973 (cf. Sect. 4.3). Because of differences between Central England and Paris temperatures (*cf.* Sect 2.2; contributing to underestimate simulated flow by a maximum of 7.5%), seasonal averages of simulated river flow have been adjusted according to the calculated mean error (ME; winter: -112.5 $m^3.s^{-1}$; spring: 6.3 $m^3.s^{-1}$; summer: 162.8 $m^3.s^{-1}$). The goodness-of-fit between observed and simulated Paris river flows has been evaluated over the common period (1885–2009). By examining the ratio of Standard Devations (*rSD*), the simulated variability is slightly underestimated by a factor of two in winter (*rSD*: 0.47) and spring (*rSD*: 0.6). Simulated and observed variability are similar in summer (*rSD*: 1.05). The timings of simulated and observed fluctuations are very consistent in winter and spring with $R \geq 0.74$, and they are reasonably good in summer ($R = 0.58$). The agreement index, which describes additive and proportional differences in the observed and simulated means and variances, and the Volumetric Efficiency (*VE*), suggest a good match of simulated to observed Seine river flow. *RSME* and *NSE* coefficients, which are linked to the mean, have been substantially reduced in winter and spring by the mean corrections. The Kling-Gupta Efficiency (*KGE*) coefficients, which facilitate the analysis of the relative importance of its different components (correlation, bias and variability), also ensure that the bias and variability ratios are not cross-correlated.

### 3.3. Multidecadal SLP patterns and their impacts on European precipitation

To improve our understanding of the multidecadal NAO variability, multidecadal time-scale anomalies of North Atlantic SLP have been extracted using EOFs (Preisendorfer, 1988). Across the Modern period (1820 –2000 for reconstructed data or 1850–2013 for observational data), we first subtracted a linear trend from all grid points and then used a 30-year running mean to define a primitive low-pass filter over each grid point. The first-EOFs were then computed for each season and, subsequently, compared to those produced using unfiltered HadSLP2r dataset, *i.e.*, the observed seasonal NAO patterns. The statistical relationships between multidecadal anomalies in the North Atlantic SLP anomalies and in the NAO patterns were quantified with spatial and temporal correlations.

We then examined changes in the seasonal relationships between the multidecadal North Atlantic SLP anomalies (which are potentially linked to multidecadal NAO variability) and European precipitation during the Modern period. Maps of the Pearson's correlation coefficients between the 30-year running means of European precipitation and multidecadal North Atlantic SLP anomalies have been computed for each season. The degrees of freedom (DOF) in the local significance calculations at $p$ = 0.05 were adjusted using the estimated decorrelation scales. To examine whether the map is statistically distinguishable from random noise, we also calculated the field significance according to the binomial procedure developed by Livezey and Chen (1983). Note that the problem of statistical independence between reconstructions of Luterbacher *et al.* (2002) and of Pauling *et al.* (2006) mainly affected the results prior to the Modern period. These two reconstructions used the NCEP/NCAR SLP data and observed precipitation field, respectively, as predictands over the 20th century.

**4. Seasonal and multidecadal hydroclimatic variability**

**4.1 Time evolution of seasonal fluctuations**

Figure 3a shows the seasonal distribution of CET anomalies since 1659. The coldest decadal period observed at the end of the 17th century is clearly distinct from the recent warmest period of the post-1970s. This is a feature of all seasons and is also consistent with earlier studies of past European climates (*e.g.*, Luterbacher *et al*., 2004; Brádzil *et al*., 2010; Büntgen *et al*., 2011). However, between these two periods, multidecadal periods of cold anomalies and warm anomalies, which are not similarly distributed in all seasons, can be identified (Fig. 3a). For instance, cold winter anomalies are observed up to the end of the 18th century; this is followed by an increase in winter warm anomalies. In summer, multidecadal cold (19th century) and warm periods (18th and 20th centuries) alternate (Fig. 3a). This therefore highlights seasonal aspects of temperature fluctuations over the past centuries, which are also consistent with earlier studies of past European climate. Here, the transition between the LIA and the Modern period has therefore been placed in the 19th century, *i.e.,* when winter temperature begins to warm up, in accordance with other studies of European and Northern Hemisphere climate (*e.g.,* Bradley & Jones, 1993; Jones *et al*., 1998; Moberg *et al*., 2005; Ljungqvist, 2010; Büntgen *et al*., 2011).

We also identify significant temporal changes in precipitation over northern France. Measurements from the Paris Observatory show that the seasonal precipitation distribution changes from one with a pronounced summer peak at the beginning of the record in 1688 until the 1750s, to an almost uniform seasonal distribution in the 20th century (Slonosky, 2002) (Fig. 3b). The seasonal reconstruction by Pauling *et al.* (2006) overestimates winter and autumn precipitation over northern France (Figs. 3c, 4a, d). This is particularly true during the first half of the 18th century, when precipitation is estimated using the Paris observations and several English early-instrumental series as predictors (Pauling *et al*., 2006). However, as in the Paris observations, winter and spring are clearly wetter during the 20th century than during the previous two centuries (Fig. 3c).

The low winter values during part of the observed record (1688–1754) could, however, be due to imperfect measurement of snow, although the notes published in the *Mémoires* indicate that the snow was melted before being measured, which would give a reasonably accurate measurement of the liquid water content. Evaporation or sublimation loss from melted or solid snow, or reduced catch of snow due to changes in the instrument location may have contributed to the low winter values. However, to balance this, the exposed East Tower should have acted as a wind shield and snow fence, increasing the catch. It was moreover noted at the time by de la Hire (1712) that this seasonal distribution (Fig. 3), with the majority of the precipitation falling in the summer months, was considered normal.

**4.2 Changes in seasonal averages, and multiscale trend analysis**

Changes in seasonal averages and trends in precipitation were investigated for both observed and reconstructed data, and results shown in Figure 4. Average winter and spring precipitation shows several positive shifts in the mean since the mid-18th century (Fig. 4a-b). Trend analysis, using the *Sen's* slope estimator and modified Mann-Kendall test of observed and reconstructed data, reveals that winter and spring precipitation show significant positive secular trends at $p = 0.05$ since the mid-19$^{th}$ century, and even earlier for spring reconstruction (Fig. 4e-f, i-j). Since the mid-19$^{th}$ century, these secular precipitation trends seem strongly influenced by semi-secular periods of alternating increasing and decreasing trend, especially in spring (Fig. 4e-f, i-j). Since the mid-18$^{th}$ century, average summer and autumn precipitation trends are not significant, except during very wet years (Fig. 4c, d, g-h, k-l). Semi-secular periods of alternating increasing and decreasing trends are also identified in summer precipitation before the 20$^{th}$ century or, for the reconstruction, before the mid-19$^{th}$ century (Fig. 4g-k). This is less clear in autumn, and it appears only in reconstruction (Fig. 4h, l). These results are consistent with early instrumental rain-gauge records in England and northern France (Dieppois, 2013), and also with historical precipitation reconstructions for Switzerland of Pfister (1994), and Alpine precipitation reconstructions of Auer *et al*. (2005) and Casty *et al*. (2005).

We then examined whether such changes in the winter, spring and summer precipitation are associated with modifications in temperature and PE (Fig. 5). Only winter temperature, and its associated PE, shows a significant change in the mean in the mid-19$^{th}$ century (Fig. 5a), which is related to significant warming trends since the beginning of the 19$^{th}$ century (Fig. 5d-i). This trend in precipitation and temperature displays a significant positive correlation at semi- to multi-secular time-scales (Fig. 6a). According to Trenberth and Shea (2005), such a relationship dominates when the water-holding capacity of the atmosphere limits precipitation amounts in cold conditions, and warm air advection in cyclonic storms is accompanied by precipitation. For time-scales of several decades, however, this could also be consistent with atmospheric circulation changes over the North Atlantic, such as produced in winter by the NAO over northern Europe (Hurrell, 1995; Cassou *et al.*, 2004; Hurrell and Deser, 2009; Fleig *et al*., 2015).

For spring and summer, this trend and change in average temperature occurs much later, *i.e.*, in the second half of the 20th century (Fig. 5b-c, e-f, j-k). Nevertheless, winter temperature and precipitation are significantly correlated with spring precipitation at time-scales greater than 50 years (Fig. 6b, d). Meanwhile, summer precipitation is negatively correlated to winter temperature from the beginning of the 19th century (Fig. 6c). The rising trend in winter temperature and precipitation could therefore slightly influence the trend in spring precipitation, potentially *via* a persistent response to a long-term change in the winter atmospheric circulation, at least since the 19th century. Such a relationship between winter and spring hydroclimatic conditions might also involve the influence of soil moisture. According to Schär *et al.* (1999) and Rowell and Jones (2006), wetter soils associated with wetter winters could lead to higher moist static energy per unit of planetary boundary layer air, and therefore be favourable to convective precipitation in the following spring. Furthermore, secular trends in temperature and PE since the mid-19th century are modulated by semi-secular periods of alternating positive and negative trends in all seasons (Fig. 5 d-k). In winter and spring, these multidecadal periods in precipitation, temperature and PE are thus in-phase, *i.e.*, wet conditions associated with warm anomalies and more potential evapotranspiration, which could be consistent with NAO-like anomalies.

In summary, winter and spring trends in precipitation are detected starting from the end of the 19th century. Interestingly, the observations here contrast with changes in European precipitation seasonality revealed by a four-century-long-tree-ring isotopic record from Brittany in western France (Masson-Delmotte *et al*., 2004), which suggested drier winters and wetter summers since the beginning of the 19th century. Additionally, this hydroclimatic trend could be modulated by semi-secular or multidecadal fluctuations.

### 4.3 Multidecadal variability of seasonal averages

Dieppois *et al.* (2013) showed that observed northern France precipitation demonstrated significant variability on time-scales of 50–80 years, 16–23 years, 9–16 years and 2–8 years. In the present paper, we show that such time-scales of precipitation variability are also characterized by different periods of increasing precipitation variance, which can reveal seasonal differences in both observed and reconstructed data, especially at the multidecadal (50–80 year) scale (Fig. 7a-f). These periods of increasing variance are statistically significant at $p = 0.05$. The 50–80 year variability of observed and reconstructed precipitation increases slightly since the end of the 19$^{th}$ century in winter (Fig 7a-b) and, more significantly, in spring (Fig. 7c-d). In summer, the variance of observed and reconstructed 50–80 year fluctuations decreases throughout the 19$^{th}$ century (Fig. 7e, f). These seasonal changes in the multidecadal variability of precipitation in northern France are also identified in early-instrumental rain-gauge records in England and northern France (Dieppois, 2013), and also with historical precipitation reconstructions for Switzerland by Pfister (1994).

The wavelet spectra of average seasonal temperatures are displayed in Figure 8a-c (the same time-scale patterns are observed in PE, not shown here). The 50–80 year fluctuations emerge in the temperature series (Fig. 8a-c). Significant periods of high variance in 50–80 year temperature variability are detected before 1750 in spring and summer, and in all seasons since the end of the 19$^{th}$ century (Fig. 8a-c). In winter and spring, increasing multidecadal fluctuations in precipitation since the end of the 19$^{th}$ century could thus be associated with multidecadal fluctuations in temperature (Figs. 7, 8). As mentioned in Section 4.2, an in-phase relationship is identified, which suggests warm (cold) air advection in cyclonic storms, such as observed during positive (negative) NAO (Hurrell, 1995). Seasonal modifications of 50–80 year NAO variability have therefore been investigated using PC-based seasonal NAO indices (Fig. 8d-f). Depending on the season, different periods of increasing variance are identified in the multidecadal NAO variability (Fig. 8d-f). For instance, we identify increased multidecadal variability of the winter and spring NAO from the end of the 19$^{th}$ century. Multidecadal variability of the summer NAO significantly decreases throughout the 19$^{th}$ century in tandem with multidecadal precipitation variability (Figs. 5, 7c, f). These multidecadal changes in the NAO indices at the end of the 19$^{th}$ century are also evident in the reconstructed fields of Küttel *et al*. (2010) and in the ADVICE and HadSLP2r observations.



From the end of the 19$^{th}$ century, increased multidecadal variability of precipitation and temperature is associated with similar changes in the summer and spring NAO. Multidecadal fluctuations induced by atmospheric circulation changes over the North Atlantic could therefore have substantially modulated the trends in the climatic variables over the 20$^{th}$ century. Furthermore, as shown in Figure 6, winter temperature and precipitation are positively correlated with spring precipitation at timescales greater than 50 years. This may reflect a delayed response to the long-term change in the winter atmospheric circulation, and/or soil moisture feedbacks (cf. Schär *et al.*, 1999; Rowell and Jones, 2006). This might therefore explain why multidecadal precipitation variability is more pronounced in spring.

**4.3. Impact of climate variations on Seine River flow**

As described in Section 3.2, the potential effects of secular and multidecadal changes in precipitation, temperature and PE on Seine river flow have been evaluated by hydrological modelling using GR2M, with the results displayed in Figure 9.

Simulated mean winter and spring river flows of the Seine at Paris show a positive shift at the beginning of the 20th century (Fig. 9d-e). Trend analysis reveals a very good match with the observations over the common period (*i.e.*, 1885–2009; *Corr.* $\geq 0.868$, significant at $p = 0.05$), and shows significant and positive secular trends since the second half of the 19th century (Fig. 9d-e). This is the first time that such positive trends have been identified in Seine river flow: hitherto, these had been obscured by significant variability at the multidecadal timescale (Fig. 9d-e, g-h). The multidecadal timescale of variability does indeed reveal a period of increasing variance in winter and spring since the end of the 19th century (Fig. 9g-h). This is particularly pronounced in spring using both simulated and observed Seine River flow. Spring is therefore an appropriate season to examine the effects of multidecadal fluctuations on the trend. For instance, a negative shift in the mean occurs during the 1940s and 1950s when multidecadal modulations of the trend changes sign (*i.e.*, positive to negative trends; Fig. 9b, e). In summer, simulated and observed river flows do not show any significant trends over the last centuries (Fig. 9c, f). Multidecadal fluctuations, which decrease throughout the 19th century, are also evident (Fig. 9f, i).

Significantly, this modelling show that changes affecting trends and multidecadal variability in precipitation and temperature over the last centuries are also identifiable in Seine river flow. This is also consistent with the findings of Boé and Habets (2014) who first highlighted that multidecadal variability in river flows over France were more pronounced in spring.

**5. Changes in multidecadal North Atlantic SLP variability**

**5.1. Multidecadal North Atlantic SLP anomalies and potential NAO linkages**

Figure 10 shows the multidecadal anomalies (>30-years) of reconstructed North Atlantic SLPs compared to NAO patterns from the unfiltered HadSLP2r dataset, which were all captured by the first-EOFs of each season for the Modern period.

Observed NAO patterns consist of north-south dipole anomalies, with one centre of action located over Greenland and the other centre of opposite sign spanning the subtropical latitudes of the North Atlantic (Fig. 10a-c). These are more notable in winter (~47.1% of the total variance). The subtropical centre is located between 35°N and 40°N in winter, but is displaced significantly north-eastward in spring and, especially, in summer (Hurrell and Deser, 2009; Folland *et al.*, 2009; Fig. 10a-c). In winter and spring, multidecadal anomalies of North Atlantic SLPs also display north-south dipole anomalies (Fig. 10d-e, g-h, j-k, m-n). By comparing the observed NAO patterns with multidecadal North Atlantic SLP anomalies, a slight southward shift of the winter NAO center of action is observed over the eastern region between Greenwich, London and 40°E (Fig. 10d, g, j, m). Such modifications are more pronounced in spring: a south-eastward (south-westward) shift of the Icelandic Low (Azores High) occurs in all reconstructions and observations (Fig. 10e, h, k, n).

These modifications in the North Atlantic meridional SLP gradient could therefore alter the zonal atmospheric circulation associated with the winter and spring NAO pattern. These multidecadal anomalies are indeed spatially similar to those of the observed NAO, especially in winter ($sCorr. \geq 0.90$, significant at $p = 0.05$), and, albeit with a reduce consistency between datasets, in spring ($0.18 \geq sCorr. \geq 0.72$, significant at $p = 0.05$). In addition, with the exception of ADVICE observations, these anomalies also show significant temporal correlations at $p = 0.05$ with multidecadal fluctuations extracted from NAO indices ($0.44 \geq tCorr. \geq 0.74$).

During summer, with the exception of reconstructions by Luterbacher *et al.* (2002), multidecadal anomalies display a SLP pattern centred on northeastern Europe with SLP anomalies of opposite signs over the Atlantic and North Africa (Fig. 10f, i, l, o). These multidecadal summer anomalies are thus unlikely to be related to the NAO ($0.01 \leq sCorr. \leq 0.31$; $-0.05 \leq tCorr. \leq 0.34$). According to the CWT of NAO index (Fig. 8f), this describes a weakening in the summer NAO multidecadal variability during the Modern period (Fig. 10f, i, l, o).

The multidecadal anomalies of North Atlantic SLPs reveal changes, which are likely to alter the NAO patterns, especially in winter and spring. Such multidecadal modulations of the NAO might be expected to be associated with changes in North Atlantic storm tracks. This will also influence northwestern European hydroclimatic conditions (cf. Section 4).

### 5.3. Multidecadal correlation patterns

By computing the correlation between 30-year running mean of precipitation and the multidecadal North Atlantic anomalies and comparing them with correlation patterns between unfiltered datasets (Fig. 11), we can now examine how North Atlantic multidecadal variability has affected seasonal relationships between the NAO and northwestern European precipitation.

The NAO patterns are associated with changes in the intensity and location of the North Atlantic jet stream and storm tracks; such large-scale modulations of the normal patterns of zonal and meridional moisture transport can modify precipitation patterns (Hurrell, 1995; Hurrell and Deser, 2009; Folland *et al.*, 2009). This is likely, then, to explain the statistically significant connection between the NAO and European precipitation during each season. The correlation patterns are characterized by a strong north-south dipole in precipitation, which is associated with wet and dry conditions over northwest Europe and the Mediterranean region, respectively, during the positive phase of the winter NAO (Fig. 11a). In spring and summer, this north-south dipole in precipitation is shifted northeastwards in response to seasonal displacements of NAO patterns (Fig. 11b-c). In all seasons, the positive phase of the NAO is usually negatively correlated with precipitation in northern France (Fig. 11a-c). This connection, however, is more pronounced in summer, when anticyclonic conditions, which are displaced northeastward, suppress precipitation in northern France.

In winter and spring, there are statistically significant connections between the multidecadal North Atlantic SLP anomalies, which are significantly linked to the NAO (Section 5.2), and European precipitation in winter and spring ($p$-Field < 20% in reconstructions and observations; Fig. 11d-e, g-h, j-k, m-n). However, during summer, with the exception of ADVICE observations, the map is indistinguishable from random noise ($p$-Field > 20% in reconstructions and observations; Fig. 11f, i, l, o). This multidecadal variability modulating the winter NAO is associated with dipole anomalies in precipitation (Fig. 11d-e, g-h, j-k, m-n). Positive anomalies of the multidecadal North Atlantic SLP variability lead to wet conditions over Scandinavia, the Baltic countries, the British Isles and the Netherlands, while they are associated with dry conditions over the Mediterranean regions. This is very similar to precipitation anomalies induced by the observed NAO, but we note positive correlations (only significant in the HadSLP observations) in northern France (Fig. 11d-e, g-h, j-k, m-n).

This suggests a southward shift in the winter NAO pattern, which might alter the westerly storm tracks at the multidecadal time-scale. Such a shift in precipitation response to changes in the multidecadal North Atlantic SLP variability is more pronounced in spring (Fig. 11e, h, k, n), when a south-eastward (south-westward) shift of the Icelandic Low (Azores High) occurs in all reconstructions and observations. A substantial shift of the NAO pattern, which might alter the westerly tracks, is also suggested at the multidecadal time-scales for spring. In spring, the multidecadal correlation patterns are indeed regionally reversed compared to that of the spring NAO. Significant positive correlations are identified over France and central-eastern Europe (Fig. 11e, h, k, n).

**6. Discussion and conclusion**

This study has defined, through detailed statistical analysis, the magnitude and direction of seasonal trends and shifts, over the last 500 years, in key hydroclimatic variables of northern France. It has also identified, especially through X and Y approaches, important potential multidecadal modulations that can themselves be driven by large-scale atmospheric variability. The evidence presented here shows that substantial changes have occurred over the past few centuries in the hydroclimate of northern France. In particular, several positive shifts and an overall increasing trend are particularly noticeable in winter and spring precipitation since the mid-19$^{th}$ century. This is linked quantitatively to rising winter temperatures during the same period.

In addition, hydrological modelling has shown that hydroclimatic trends have helped to drive significant increases in mean Seine river flows at Paris, but only in winter and spring. Further work will address additional drivers of river flow variations over the past five centuries related to geomorphological changes in the watershed, and/or modifications in the catchment properties associated with land use changes, such as forest clearance, shifts to arable farming, increasing viticulture (especially in the Champagne region of eastern part of the Seine basin), as well as social landholding fragmentation (dismemberment) processes which were very common in France, but which are now being addressed through "rememberment" initiatives. Such land use changes elsewhere have typically led to reductions in infiltration rates, increased runoff, enhanced sediment losses from catchment slopes to river channels, and declines in groundwater recruitment and storage.

Nevertheless, we have found that such secular trends in the seasonal hydroclimatic conditions over northern France are actually associated with key multidecadal fluctuations. Indeed, increasing variance of hydroclimatic multidecadal variability since the end of the 19$^{th}$ century has emerges strongly, but mainly/only in winter and spring seasons.

Such multidecadal hydrological fluctuations are driven mainly by large-scale circulation changes. Similar connections have been previously revealed for eastern North American and UK hydrosystems (Phillips *et al*., 2003; Dixon *et al*., 2006; Kingston *et al*., 2006a, b, 2009, 2011; Lavers *et al*., 2010; Holman *et al*., 2011). However, these have been for much shorter periods than the 500 years here. Also the more complex and exhaustive analyses here have substantially extended understanding of these hydroclimatic fluctuations and their circulation drivers into a new key region of North Atlantic, Europe and northern France (cf. Massei *et al*., 2007).

Our results also demonstrate how North Atlantic multidecadal variability, which arises principally from internally generated natural processes, are likely to influence recent trends (or lack thereof) in hydroclimatic variables, and which are very likely to contribute to future climate variability (Keenlyside *et al.*, 2008; Watanabe *et al.*, 2014). Multidecadal NAO variability has increased since the 19$^{th}$ century in winter and spring.

Furthermore, multidecadal anomalies of North Atlantic SLPs since the 19th century reveal changes in the meridional dipole, which are statistically linked to modulations of the NAO. In particular, in spring, a south-eastward (south-westward) shift of the Icelandic Low (Azores High) drives significant multidecadal hydroclimatic changes: this leads to modulations of moisture advection in response to shifts of North Atlantic storm tracks over European regions, and wetter springs in northern France during positive NAO phases. Similar changes are observed in winter, although these are less pronounced.

Recently, based on the results from CCSM4 model, Sun *et al.* (2015) proposed two possible mechanisms responsible for the multidecadal variability of the NAO: the forcing of the Atlantic Multidecadal Oscillation (AMO; Knight *et al.*, 2005) by the NAO, and delayed negative feedback exerted by the AMO. At the same time, as proposed by Franckombe *et al.* (2010), the North-Atlantic multidecadal variability is also related to exchange processes between the Atlantic and Arctic Oceans. This idea is consistent with the work of Miles *et al.* (2014) who identify concomitant reinforcement of multidecadal variability in the AMO and several Arctic sea-ice indices at the end of the 19th century. Also, it is possible that anomalous sea-ice and freshwater pulses through Fram Strait could have helped to drive, as presented here, an eastward shift in the Iceland Low over recent decades (Hilmer and Jung, 2000). Intriguingly, this could thus form a hitherto unrecognized but fundamental and interactive component of multidecadal North Atlantic variability in the post-LIA period, and consequently affect multidecadal variability of hydrosystems in France and over NW Europe more generally. This requires testing in future work.

The possible influence of an early warming winter temperature over the Arctic regions on Arctic sea-ice export, which has been detected here in central England and Paris (not shown), should be explored very carefully (see, *e.g*., Slonosky *et al.* (1997) and Mysak *et al*. (1996) for multidecadal sea-ice and atmospheric circulation anomalies in the 20$^{th}$ century). This might have played a role in initiating increased multidecadal climate variability over the North Atlantic. External forcing could also be involved in the relationship between North Atlantic multidecadal variability and European hydroclimatic variability. Recently, Knudsen *et al.* (2014) suggested that external forcing, *i.e*., solar variability or volcanic forcing, played a dominant role in pacing the AMO after termination of the LIA. Also, anthropogenic and natural aerosols have likely played some role in forcing the Atlantic multidecadal variability (Chang *et al*., 2011; Booth *et al*., 2012; Villarini and Vecchi, 2013).

Our study also demonstrates that warming trends began earlier than hitherto recognised, which are associated with changes in PE, precipitation and, potentially, in river flow in a major European hydroclimatic system (northern France and the Seine river basin). Until now, these trends were masked by aperiodic multidecadal oscillations that originated from internal variability in the North Atlantic climate system. Although this could involve non-linear and chaotic interactions, which are not yet well understood, the impact of such multidecadal oscillations on hydroclimate in northern France seems as important as the secular trends since the mid-19$^{th}$ century. Understanding future regional and continental hydroclimatic trends, especially precipitation and river flow over the next 50 years is a challenge. However, it is likely that illumination of this key question could be driven by improved knowledge of the links between North Atlantic multidecadal climatic variability and hydrological impacts over the European continent.

**Acknowledgements.** The authors would like to thank the Upper Normandy regional research federation FED 4116 SCALE for financial support.

## References

Aksoy H, Gedikli A, Unal E, Kehegias A. 2008. Fast segmentation algorithms for long hydrometeorological time series. *Hydrological Processes* **22:**4600–4608.

Allan R, Ansell T. 2006. A new globally complete monthly historical gridded mean sea level pressure data set (HadSLP2): 1850-2004. *Journal of Climate* **19:**5816–5842.

Auer I, Böhm R, Jurkovic A, Orkik A, Potzmann R, Schöner W, Ungerböck W, Ungersböck M, Brunetti M, Nanni T, Maugeri M, Briffa K, Jones PD, Elfthymiadis D, Mestre O, Moisselin JM, Begert M, Bradzil R, Bochnice O, Cegnar T, Gajic-Capka M, Zaninovic K, Majstorovic Z, Szalai S, Szentimrey T, Mercalli L. 2005. A new instrumental precipitation dataset for the greater Alpine region for the period 1800–2002. *International Journal of Climatology* **25:**139–166.

Boé J, Habets F. 2014. Multi-decadal river flow variations in France. *Hydrology and Earth System Sciences* **18:**691–708.

Booth BBB, Dunstone NJ, Halloran PR, Andrews T, Bellouin N. 2012. Aerosols implicated as a prime driver of twentieth-century North Atlantic climate variability. *Nature* **484:**228–232.

Bradley RS, Jones PD. 1993. 'Little ice age' summer temperature variations: their nature and relevance to recent global warming trends. *The Holocene* **3:**367–376.

Brádzil R, Dobrovný P, Luterbacher J, Moberg A, Pfister C, Wheeler D, Zorita E. 2010. European climate of the past 500 years: new challenges for historical climatology. *Climatic Change* **101:**7–40.

Büntgen U, Tegel W, Nicolussi K, McCormick M, Frank D, Trouet V, Kaplan JO, Herzig F, Heussner K-U, Wanner H, Luterbacher J, Esper J. 2011. 2500 years of European climate variability and human susceptibility. *Science* **331:**578–582.

Büntgen U, Hellmann L. 2014. The Little Ice Age in scientific perspective: cold spells and caveats. *Journal of Interdisciplinary History* **44:**353–368.

Cassou C, Terray L, Deser C. 2004. North Atlantic winter climate regimes: spatial asymmetry, stationarity with time oceanic forcing. *Journal of Climate* **17:**1055–1068.

Casty C, Wanner H, Luterbacher J, Esper J, Böhm R. 2005. Temperature and precipitation variability in the European Alps since 1500. *International Journal of Climatology* **25:**1855–1880.

Chang CY, Chiang JCH, Wehner MF, Friedman AR, Ruedy R. 2011. Sulfate aerosol control of tropical Atlantic climate over the twentieth century. *Journal of Climate* **24:**2540–2555.

Cook ER, D'Arrigo RD, Briffra KR. 1998. A reconstruction of the North Atlantic Oscillation using tree-ring chronologies from North America and Europe. *Holocene* **8:**9–17.

Dawson AG, Elliot L, Mayewski P, Lockett P, Noone S, Hickey K, Holt T, Wadhams P, Foster I. 2003. Late-Holocene North Atlantic climate 'seesaws', storminess changes and Greenland ice sheet (GISP2) palaeoclimates. *The Holocene* **13**(3):381–392.

Dawson AG, Hickey K, Mayewski PA, Nesje A. 2007. Greenland (GISP2) ice core and historical indicators of complex North Atlantic climate changes during the fourteenth century. **The Holocene** *17*(4):427–434.

De la Hire P. 1712. Observations sur la pluye, sur le Thermomètre et sur le Baromètre, à l'Observatoire Royal pendant l'année 1711. *Mémoires de l'Académine Royale des Sciences,* **1712:**1–5.

Dieppois B. 2013. *Nonstationnary teleconnexions of Atlantic low-frequency oscillations and the regional climates of NW Europe (1700–2010) and West African Sahel (1900–2010)*. PhD dissertation, University of Rouen, Mont-Saint Aignan, France.

Dieppois B, Durand A, Fournier M, Massei N. 2013. Links between multidecadal and interdecadal climatic oscillations in the North Atlantic and regional climate variability of northern France and England since the $17^{th}$ century. *J Geophys Res (Atmos)* **118:**4359–4372.

Dixon H, Lawler DM, Shamseldin AY. 2006. Streamflow trends in western Britain. *Geophys Res Lett* **33:**L19406, doi: 10.1029/2006GL027325.

Dong B, Sutton RT, Woolings T. 2011. Changes of interannual NAO variability in response to greenhouse gases forcing. *Climate Dynamics* **37:**1621–1641.

Droogers P, Allen RG. 2002. Estimating reference evapotranspiration under inaccurate data conditions. *Irrigations and Drainage Systems* **16:**33–45.

Folland CK, Knight J, Linderholm W, Fereday D, Ineson S, Hurrell JW. 2009. The summer North Atlantic Oscillation: past, present, and future. *Journal of Climate* **22:**1082–1103.

Fleig AK, Tallaksen LM, James P, Hisdal H, Stahl K. 2015. Attribution of European precipitation and temperature trends to changes in synoptic circulation. *Hydrol Earth Syst Sci* **19:**3093–3107.

Franckombe LM, von der Heydt A, Dijkstra HK. 2010. North Atlantic Multidecadal Climate Variability: An Investigation of Dominant Time Scales and Processes. *Journal of Climate* **23:**3626–3638.

Franke J, Frank D, Raible CC, Esper J, Brönnimann S. 2013. Spectral biases in tree-ring climate proxies. *Nature Climate Change* **3:**360–364.

Fritier N, Massei N, Laignel B, Durand A, Dieppois B, Deloffre J. 2012. Links between NAO fluctuations and inter-annual variability of winter months precipitation in the Seine River watershed (north-western France). *C R Geoscience* **344:**396–405.

Gamiz-Fortis SR, Pozo-Vasquez D, Trigo RM, Castro-Diez Y. 2008. Quantifying the predictability of winter river flow in Iberia. Part I: Interannual predictability. *Journal of Climate* **21:**2484–2502.

Goodkin NF, Hughen KA, Doney SC, Curry WB. 2008. Increased multidecadal variability of the North Atlantic Oscillation since 1781. *Nature Geoscience* **1:**844–848.

Grove JM. 1988. *The Little Ice Age*. Methuen, London. 498p.

Hamed KH, Rao AR. 1998. A modified Mann Kendall trend test for autocorrelated data. *Journal of Hydrology* **204:**182–196.

Hargreaves GH. 1994. Defining and using reference evapotranspiration. *J Irrig and Drain Engrg, ASCE* **120:**1132–1139.

Hilmer M, Jung T. 2000. Evidence for a recent change in the link between the North Atlantic Oscillation and Artic sea ice export. *Geophys Res Lett* **27:** 989–992.

Holman IP, Rivas-Casado M, Bloomfield JP, Gurdak JJ. 2011. Identifiying non-stationary groundwater level response to North Atlantic ocean-atmosphere teleconnection patterns using wavelet coherence. *Hydrol J* **19:**1269–1278.

Hurrell JW. 1995. Decadal trends in the North Atlantic climate variability: Regional temperatures and precipitation. *Science* **269:**676–679.

Hurrell JW, Deser C. 2009. North Atlantic climate variability: the role of the North Atlantic Oscillation. *J Mar Syst* **78:**28–41.

Ineson S, Scaife AA, Knight JR, Manners JC, Dunstone NJ, Gray LJ, Haigh J. 2011. Solar forcing of winter climate variability in the Northern Hemisphere. *Nature Geoscience* **4:**753–757.

Jansen E, et al. 2007. *Palaeoclimate. In: Climate Change 2007: The Physical Science Basis. Contribution of Working Group I to the Fourth Assessment Report of the Intergovernmental Panel on Climate Change* [Solomon S, Qin D, Manning M, Chen Z, Marquis M, Averyt KB, Tignor M, Miller HL (eds)]. Cambridge University Press, Cambridge, p 433–497.

Jones PD, Briffa KR, Barnett TP, Tett SFB. 1998. High-resolution palaeoclimatic records for the last millennium: interpretation, integration and comparison with general circulation model control run temperatures. *Holocene* **8:**477– 483.

Jones PD, Davies TD, Lister DH, Slonosky V, Jönsson T, Bärring L, Jönsson P, Maheras P, Kolyva-Machera F, Barriendos M, Martin-Vide J, Alcoforado MJ, Wanner H, Pfister C, Schuepbach E, Kaas E, Schmith T, Jacobeit J, Beck C. 1999. Monthly mean pressure reconstructions for Europe. *International Journal of Climatology* **19:**347–364.

Jung T, Hilmer M, Ruprecht E, Kleppek S, Gulev S, Zolina O. 2003. Characteristics of the recent eastward shift of interannual NAO variability. *Journal of Climate* **16***:*3371–3382.

Keenlyside NS, Latif M, Jungclaus J, Kornblueh L, Roeckner E. 2008. Advancing decadal-scale climate prediction in the North Atlantic sector. *Nature* **453:**84–88.

Kingston DG, Lawler DM, McGregor GR. 2006a. Linkages between atmospheric circulation, climate and streamflow in the northern North Atlantic: research prospects *Progress in Physical Geography, 30*, 2, 143–174.

Kingston DG, McGregor GR, Hannah DM, Lawler DM. 2006b. River flow teleconnections across the northern North Atlantic region. *Geophys Res Lett* **33:**L14705, doi :10.1029/2006GL026574.

Kingston DG, McGregor GR, Hannah DM, Lawler DM. 2007. Large-scale climatic controls on New England River Flow, *J Hydrometeor* **8:**367–379.

Kingston DG, Hannah DM, Lawler DM, McGregor GR. 2009. Climate-river flow relationships across montane and lowland environments in northern Europe. *Hydrological Processes* **23:**985–996.

Knight JR, Allan RJ, Folland CK, Vellinga M, Mann ME. 2005. A signature of persistent natural thermohaline circulation cycles in observed climate. *Geophys Res let* **32:**L20708, doi:10.1929/2005GL024233.

Knudsen MF, Jacobsen BH, Seidenkrantz M-S, J Olsen .2014. Evidence for external forcing of the Atlantic Multidecadal Oscillation since termination of the Little Ice Age. *Nature Communications* **5:**3323,doi:10.38/ncomms4323.

Küttel M, Xoplaki E, Gallego D, Luterbacher J, Garcia-Herrera R, Allan R, Barriendos M, Jones PD, Wheeler D, Wanner H. 2010. The importance of ship log data: reconstructing North Atlantic, European and Mediterranean sea level pressure fields back to 1750. *Climate Dynamics* **34:**1115–1128.

Lavers D, Prudhomme C, Hannah DM. 2010. Large-scale climatic influences on precipitation for a British river basin. *Hydrological Processes* **24:**2555–2653.

Lawler DM. 1987. *Climatic change over the last millennium in Central Britain*. *In: Paleohydrology in Practice: a river basin analysis* [Gregory KJ, Lewin J, Thornes JB (eds.)]. John Wiley and Sons Ltd. 99–129.

Lehner F, Raible C, Stocker TF. 2012. Testing the robustness of a precipitation proxy-based North Atlantic Oscillation reconstruction*.* *Quaternary Science Reviews* **45:**85–94.

Liebman B, Dole RM, Jones C, Bladé C, Allured D. 2010. Influence of choice of time period on global surface temperature trend estimates*.* *Bull Amer Meteor Soc* **91:**1485–1491.

Livezey RE, Chen MY. 1983. Statistical field significance and its determination by Monte Carlo techniques. *Mon Wea Rev* **111:**46–59.

Ljungqvist FC. 2010. A new reconstruction of temperature variability in the extra-tropical Northern Hemisphere during the last two millennia. *Geogr Ann* **92:**339–351.

Luterbacher J, Schmutz C, Gyalistras D, Xoplaki E, Wanner H. 1999. Reconstruction of monthly NAO and EU indices back to AD 1675. *Geophys Res Lett* **26:**2745–2748.

Luterbacher J, Xoplaki E, Dietrich D, Rickly R, Jacobeit J, Beck C, Gyalistras D, Schmutz C, Wanner H. 2002. Reconstruction of sea level pressure fields over the eastern north Atlantic and Europea back to 1500. *Climate Dynamics* **18:**545–561.

Luterbacher J, Dietrich D, Xoplaki E, Grosjean M, Wanner H. 2004. European seasonal and annual temperature variability, trends, and extremes since 1500. *Science* **303:**1499–1503.

Manley G. 1974. Central England Temperatures: monthly means 1659 to 1973. *QJR Meteorol Soc* **100:**389–405.

Mann ME, Zhang ZH, Rutherford S, Bradley RS, Hughes MK, Shindell D, Ammann C, Faluvegi G, Ni FB. 2009. Global signatures and dynamical origins of the Little Ice Age and Medieval Climate Anomaly. *Science* **326**(5957):1256-1260.

Maraun D. 2006. *What can we learn from climate data? Methods for fluctuation time/scale and phase analysis.* PhD thesis, University of Postdam, Germany.

Massei N, Durand A, Deloffre J, Dupont JP, Valdes D, Laignel B. 2007. Investigating possible links between the North Atlantic Oscillation and precipitation variability in northwestern France over the past 35 years. *J Geophys Res (Atmos)* **112:**D09121, doi:10.1029/2005JD07000.

Masson-Delmotte V, Raffalli-Delerce G, Danis PA, Yiou P, Stienvenard M, Guibal F, Mestre O, Bernard V, Goose H, Hoffman G, Jouzel J. 2005. Changes in European precipitation seasonality and in drought frequencies revealed by a four-century-long tree-ring isotopic record from Brittany, western France. *Climate Dynamics* **24:**57–69.

McCabe GJ, Wolock DM. 2002. A step increase in streamflow in the conterminous United States. *Geophys Res let* **29:**2185, doi:10.1029/2002GL015999.

Meeker L, Mayewski P. 2002. A 1400-year high-resolution record of atmospheric circulation over the North Atlantic and Asia. *The Holocene* **12:**257–266.

Miles MW, Divine DV, Furevik T, Jansen E, Moros M, Ogilvie AEJ. 2014. A signal of persistent Atlantic multidecadal variability in Arctic sea ice. *Geophys Res Lett* **41:**463–469.

Moberg A, Sonechkin DM, Holmgren K, Datsenko NM, Karlén W. 2005. Highly variable Northern Hemisphere temperatures reconstructed from low- and high-resolution proxy data. *Nature* **433:**613–617.

Mouelhi S, Michel C, Perrin C, Andréassian V. 2006. Stepwise development of a two-parameter monthly water balance model. *Journal of Hydrology* **318:**200–214.

Mysak L, Ingram RG, Wang J and van der Baaren A. 1996. The anomalous sea ice extent in Hudson Bay, Baffin Bay and the Labrador Sea during three simultaneous ENSO and NAO episodes. *Atmosphere-Ocean* **34:**313-343.

Olsen J, Anderson NJ, Knudsen MF. 2012. Variability of the North Atlantic Oscillation over the past 5,200 years. *Nature Geoscience* **5:**808–812.

Parker DE, Legg TP, Folland CK. 1992. A new daily Central England Temperature Series, 1772-1991. *International Journal of Climatology* **12:**316–342.

Pauling A, Luterbacher J, Casty C, Wanner H. 2006. 500 years of gridded high resolution precipitations over Europe and the connection to large-scale circulation. *Climate Dynamics* **26:**387–405.

Pfister C. 1994. *Spatial patterns of climatic change in Europe 1675–1675. In: Climatic trends and anomalies in Europe 1675–1715* [Frenzel, B., Pfister, C., Gläser, B. (eds)]. Gustav Fischer, Stuttgart, 205–224.

Philips ID, McGregor GR, Wilson CJ, Bower D, Hannah DM. 2003. Regional climate and atmospheric circulation controls on the discharge of two British rivers, 1974–97, *Theoretical and Applied Climatology* **76:**141–164.

Preisendorfer RW. 1988. *Principal Component Analysis in Meteorology and Oceanography*, Elsevier, Amsterdam, 425 pp.

Raible CC, Casty C, Luterbacher J, Pauling A, Esper J, Frank DC, Buentgen U, Roesch AC, Tschuck P, Wild M, Vidale PL, Schaer C, Wanner H. 2006. Climate variability-observations, reconstructions, and model simulations for the Atlantic European and Alpine region from 1500–2100 AD. *Climatic Change* **79**:9–29.

Raible CC, Lehner F, Gonzales-Rouco JF, Fernandez-Donado L. 2014. Changing correlation structures of the Northern Hemisphere atmospheric circulation from 1000 to 2100 AD. *Climate of the Past* **10:**537–550.

Renou E. 1885. *Etude sur le climat de Paris, 2e Partie: la pluie depuis 1688*. Annales du Bureau central météorologique, Paris, 259–277.

Rowell DP, Jones RG. 2006. Causes and uncertainty of future summer drying over Europe. *Climate Dynamics* **27:**281–299.

Sang YF. 2013. A review on the applications of wavelet transform in hydrology time series analysis. *Atmospheric Research* **122***:*8–15.

Schär C, Lüthi D, Beyerle U, Heise E. 1999. The soil-precipitation feedback: A process study with a regional climate model. *Journal of Climate* **12**:722–741.

Sen PK. 1968. Estimates of the regression coefficient based on Kendall's tau. *J Am Statist Assoc* **63:**1379–1389.

Sheffield J, Wood EF, Roderick ML. 2012. Little change in global drought over the past 60 years. *Nature* **491:**435–438.

Slonosky VC, Mysak LA, Derome J. 1997. Linking Arctic sea-ice and atmospheric circulation anomalies on interannual and decadal timescales. *Atmosphere-Ocean* **35**:333–336.

Slonosky VC. 2002. Wet winters, dry summers? Three centuries of precipitation data from Paris. *Geophys Res Lett* **19**:1895, doi:10.1029/2001GL014302.

Slonosky VC, Jones PD, Davies TD. 2001. Instrumental pressure observations and atmospheric circulation from the 17th and 18th centuries: London and Paris. *International Journal of Climatology* **21:**285–298.

Slonosky VC, Yiou P. 2002. Does the NAO index represent zonal flow? The influence of the NAO on North Atlantic surface temperature. *Climate Dynamics* **19**(1):17–30.

Sun C, Li J, Jin FF. 2015. A delayed oscillator model for the quasi-periodic multidecadal variability of the NAO. *Climate Dynamics* **published online:** doi 10.1007/s00382-014-2459-z.

Tabony RC. 1980. *A set of homogeneous European precipitation series*, Met. O13 Branch Memorandum No. 104, Meteorological Office, Bracknell.

Tabony RC. 1981. A principal component and spectral analysis of European precipitation. *J climatol* **1:**283–294.

Thornthwaite CW. 1948. An approach toward a rational classification of climate. *Geographical Review* **38:**55–94.

Torrence C, Compo GP. 1998. A practical guide to wavelet analysis. *Bull Am Meteorol Soc* **79:**61–78.

Trenberth KE, Shea DJ. 2005. Relationships between precipitation and surface temperature. *Geophys Res let* **32:**L14703, doi :10.11029/2005GL022760.

Trouet V, Esper J, Graham NE, Baker A, Scourse JD, Frank DC. 2009. Persistent positive North Atlantic Oscillation mode dominated the Medieval Climate Anomaly. Science 324(5923):78–80.

Trouet V, Scourse JD, Raible CC. 2012. North Atlantic storminess and Atlantic Meridional Overturning Circulation during the last Millenium : Reconciling contradictory proxy records of NAO variability. Global and Planetary Change 84–85:48–55.

van Loon H, Brown J, Milliff RF. 2012. Trends in sunspots and North Atlantic sea level pressure. *J Geophys Res (Atmos)* **17:**D07106, doi:10.1029/2012JD017502.

Villarini G, Vecchi GA. 2013. Projected increases in North Atlantic tropical cyclone intensity from CMIP5 models. *Journal of Climate* **26:**3231–3240.

Watanabe M, Shiogama H, Tatebe H, Hayashi M, Ishii M, Kimoto M. 2014. Contribution of natural decadal variability to global warming acceleration and hiatus. *Nature Climate Change* **4:**893–897.

Xoplaki E, Luterbacher J, Paeth H, Dietrich D, Steiner N, Grosjean M, Wanner H. 2005. European spring and autumn temperature variability and changes of extremes over the last half millennium. *Geophys Res Lett* **32:**L15713, doi:10.1029/2005GL23424.

## List of Figures

Figure 1. Overview of the data sets used in this study against time-scale. Observation and reconstruction data are indicated in blue and orange, respectively. Time series and gridded data are displayed in lines and boxes, respectively. Time series derived from calculations are in red.

Figure 2. Spatial coherence of each seasonal precipitation time series. (a-d) Seasonal pointwise correlations precipitation anomalies of observed Paris rain-gauges and the CRU TS 3.10.1 field over the NW Europe (top: DJF; top center: MAM, bottom center: JJA, bottom: SON). (e-h) As in (a-d) using a reconstructed northern France precipitation index (47.5 – 50.5°N; 0 – 4°E) and the high-resolution precipitation reconstruction of Pauling *et al.* (2006). Red contours indicate correlations significant at the 95% confidence level (p<5%).

Figure 3. Temporal evolution of seasonal distributions of temperature and precipitation in northern France. (a) Observed secular distributions of monthly Central England Temperature anomalies (°C) with regard to the $20^{th}$ century mean (red: warm anomalies; blue: cold anomalies). (b) Observed secular distributions of monthly Paris precipitation ($mm.month^{-1}$) since 1700. (c) As in (b) for a seasonal reconstructed northern France precipitation index ($mm.season^{-1}$) since 1500. Grey contours delineate the area above which precipitation is greater than the multi-decadal mean (~60 year smoothing window).

Figure 4. Modifications in mean and trend of seasonal precipitation amounts in northern France over the last five centuries. (a-d) Multiples changes of the means in the observed (grey) and reconstructed (light red) seasonal precipitation time series (mm.season$^{-1}$; winter: DJF; spring: MAM; summer: JJA; autumn: SON). Bold lines display optimal breaks between adjacent segments with means that are significantly different from the *Scheffe* contrast test at the 95% confidence interval as determined by a segmentation procedure. (e-h) Two-dimensional diagrams of every possible trend in the observed seasonal precipitation time series as determined by a modified Mann-kendall test. Trend strength (positive: blue; negative: red) is estimate using the *Sen's* slope while statistical significance at $p$ = 0.05 (contour) is assumed by the two-sided *p-values*. (i-l) As in (e-h) for a seasonal reconstructed northern France precipitation index (mm.season$^{-1}$) since 1500.



Figure 5. Modifications in mean and trend of seasonal central England temperature and its associated evapotranspiration (PE) over the last centuries. (a-c) Multiples changes of the means in observed temperature (°C; grey) and PE (mm; light red) winter: DJF; spring: MAM; summer: JJA). Bold lines display optimal breaks between adjacent segments with means that are significantly different from the *Scheffe* contrast test at the 95% confidence interval as determined by a segmentation procedure. (d-f) Two-dimensional diagrams of every possible trend in observed temperature as determined by a modified Mann-kendall test. Trend strength (positive: red; negative: blue) is estimate using the *Sen's* slope while statistical significance at $p$ = 0.05 (contour) is assumed by the two-sided *p-values*. (g-k) As in (e-h) for PE (positive: blue; negative: red) since 1500.

Figure 6. Time-scale evolution of relationships between winter temperature/precipitation and seasonal precipitation average. (a-c) Two-dimensional diagrams of every possible correlation between winter temperature and winter precipitation (at the top), spring precipitation (at the middle) and summer precipitation (at the bottom). (d-e) as for (b-c) but for the correlation between winter precipitation and spring and summer precipitation. Contours indicate correlations statistically significant at $p = 0.05$ of Pearson's product moment correlation coefficient assuming independent normal distributions. Note that the degrees of freedom (DOF) in the significance calculations are adjusted using the estimated decorrelation scales.

Figure 7. Time-scale patterns of variability in the seasonal precipitation amounts of northern France. (a-f) Wavelet power spectrum of observed (left column) and reconstructed (right column) seasonal precipitation time series (winter: DJF; spring: MAM; summer: JJA). The very thick bold lines (the so-called cone of influence) delineates the area under which power can be underestimated as a consequence of edge effects, wraparound effects and zero padding; thin contour lines show the 95% confidence limits based on 1000 Monte-Carlo simulations of the red noise background spectrum. Note that these time-scale patterns were also obtained without padded with zeroes near the edge of the time series.

Figure 8. Time-scale patterns of variability in seasonal temperature (and PE) and in the NAO indices. (a-c) Wavelet power spectra of seasonal central England temperature (CET; °C), which are similar to those of PE (winter: DJF; spring: MAM; summer: JJA). (d-f) as in (a-c) for the PC-based seasonal NAO indices. The very thick bold lines (the so-called cone of influence) delineates the area under which power can be underestimated as a consequence of edge effects, wraparound effects and zero padding; thin contour lines show the 95% confidence limits based on 1000 Monte-Carlo simulations of the red noise background spectrum. Note that these time-scale patterns were also obtained without padded with zeroes near the edge of the time series.

Figure 9. Evaluation of modifications in mean, trend and decadal variability of Paris river flow by GR2M hydrological modelling. (a-c) Multiples changes of the seasonal means (winter: DJF; spring: MAM; summer: JJA) in observed (grey lines) and simulated Paris river flow (red lines; $m^3.s^{-1}$). Bold lines display optimal breaks between adjacent segments with means that are significantly different from the *Scheffe* contrast test at the 95% confidence interval as determined by a segmentation procedure. The light blue boxes indicate goodness-of-fit measures between observed and simulated values with regard to the common period (1885–2009) before (black) and after (grey) the mean corrections. (d-f) Two-dimensional diagrams of every possible trend in seasonal observed (small box) and simulated river flow as determined by a modified Mann-kendall test. Trend strength (positive: blue; negative: red) is estimate using the *Sen's* slope while statistical significance at $p = 0.05$ (contour) is assumed by the two-sided *p-values*. Correlations between observed and simulated trend patterns, and their statistical significances at $p = 0.05$, over the common period are indicated on the upper right corners of the observed diagrams. (g-i) Wavelet power spectra of seasonal observed (small box) and simulated river flow. The very thick bold lines (the so-called cone of influence) delineates the area under which power can be underestimated as a consequence of edge effects, wraparound effects and zero padding; thin contour lines show the 95% confidence limits based on 1000 Monte-Carlo simulations of the red noise background spectrum.

Figure 10. Seasonal NAO patterns and multidecadal anomalies in North Atlantic SLP during the Modern period. (a-c) Seasonal 1st EOF of unfiltered North Atlantic SLP (30° – 70°N; 30°W – 40°E), *i.e.*, NAO patterns, from the HadSLP2r dataset during the modern period. (d-f) Reconstruction using EOF of multidecadal anomalies (*i.e.,* 30-year running mean) in the winter to summer observed North Atlantic SLP during the modern period. (g-l) as for (d-f) but using SLP reconstructions from Luterbacher *et al.* (2002) and Küttel *et al.* (2010). (m-o) idem based on ADVICE observation fields. Fraction of the variance expressed by each 1st EOFs are displayed on the upper right corners. Spatial and temporal correlation (*sCorr.* and *tCorr.*) between multidecadal anomalies and the NAO (*i.e.,* observed NAO patterns and multidecadal variability extracted from the NAO indices for each dataset) are indicated on the lower left corners. Asterisks indicate significant correlations at $p = 0.05$ with regard to Dutilleul's and Pearson's *t*-tests accounting for spatial and temporal autocorrelation.

Figure 11. Seasonal correlation patterns between European precipitation and the NAO, as well as the multidecadal North Atlantic SLP anomalies during the Modern period. (a-c) Pointwise correlations between seasonal PC-based NAO indices from HadSLP2r dataset and European precipitation during the Modern period. (d-f) Seasonal pointwise correlations between the 30-year running mean of European precipitation and observed multidecadal North Atlantic SLP anomalies during the Modern period. (g-l) as for (d-f) but using SLP reconstructions from Luterbacher *et al.* (2002) and Küttel *et al.* (2010). (m-o) idem based on ADVICE observation fields. Note that the degrees of freedom (DOF) in the significance calculations are adjusted using the estimated decorrelation scales, so the signal may not be more significant after the low-pass filtering. The $p$-values at the 95% (*i.e.,* $p$=0.05) confidence level are computed against a 1000 sample Monte-Carlo simulations, where the precipitation fields are replaced with red noise. Field significance and the spatial DOF are displayed on the upper right corners.

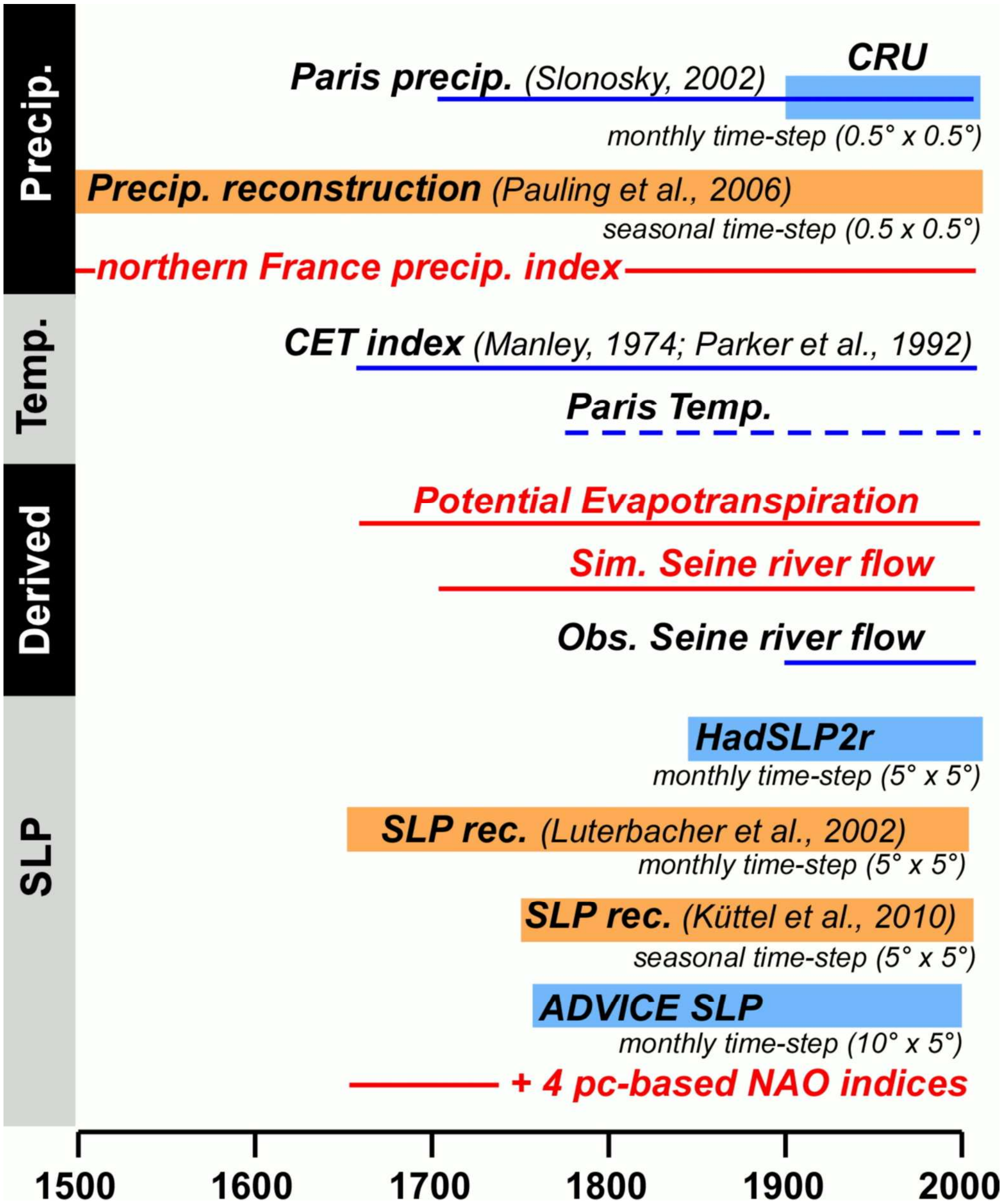


Figure 1. Overview of the data sets used in this study against time-scale. Observation and reconstruction data are indicated in blue and orange, respectively. Time series and gridded data are displayed in lines and boxes, respectively. Time series derived from calculations are in red.
219x263mm (300 x 300 DPI)

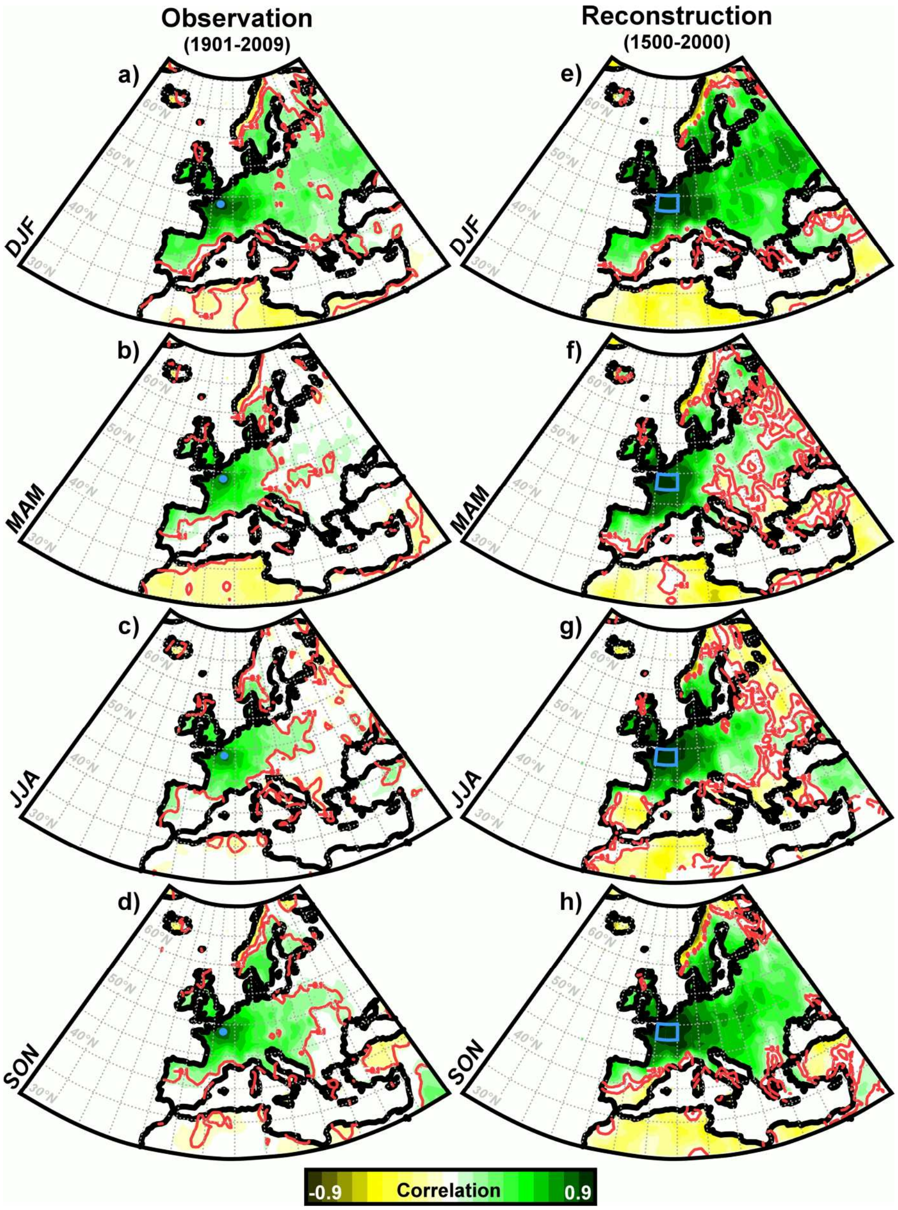


Figure 2. Spatial coherence of each seasonal precipitation time series. (a-d) Seasonal pointwise correlations precipitation anomalies of observed Paris rain-gauges and the CRU TS 3.10.1 field over the NW Europe (top: DJF; top center: MAM, bottom center: JJA, bottom: SON). (e-h) As in (a-d) using a reconstructed northern France precipitation index (47.5 – 50.5°N; 0 – 4°E) and the high-resolution precipitation reconstruction of Pauling et al. (2006). Red contours indicate correlations significant at the 95% confidence level (p<5%).
444x598mm (300 x 300 DPI)

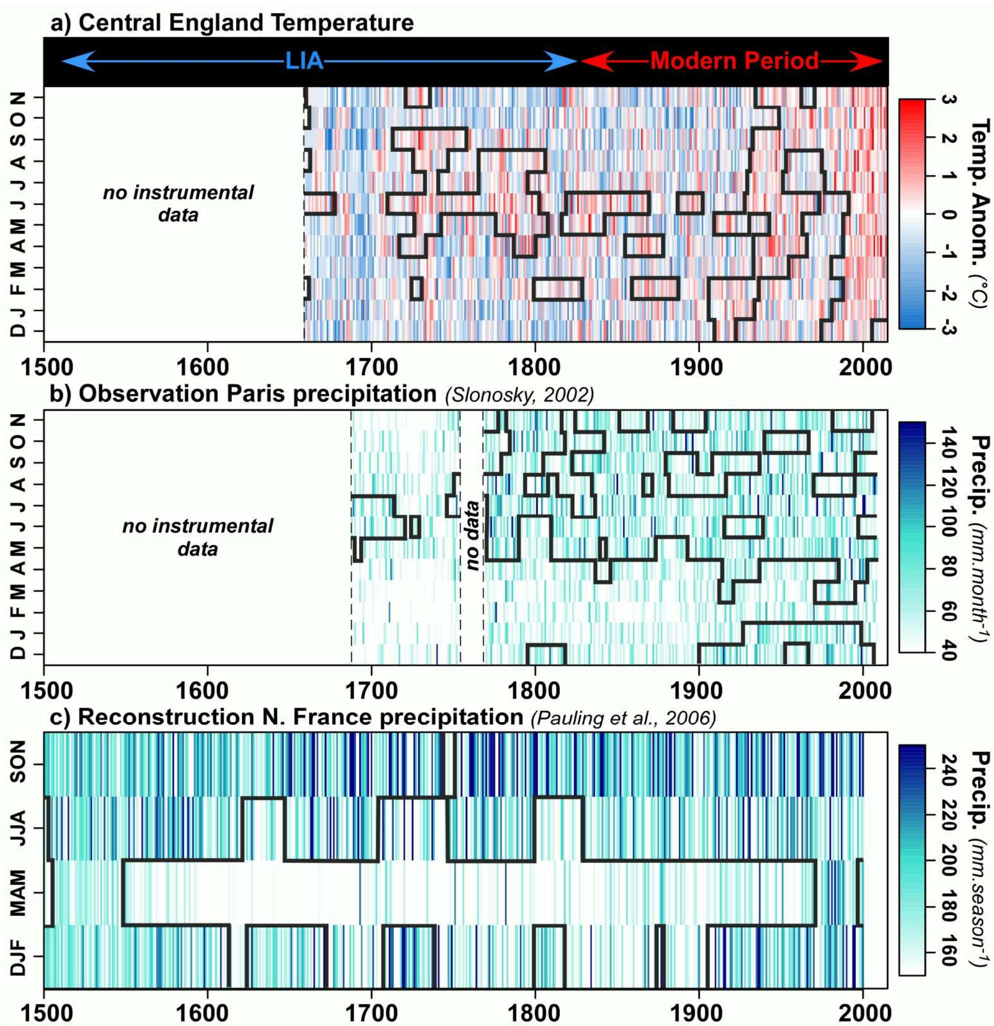


Figure 3. Temporal evolution of seasonal distributions of temperature and precipitation in northern France. (a) Observed secular distributions of monthly Central England Temperature anomalies (°C) with regard to the 20th century mean (red: warm anomalies; blue: cold anomalies). (b) Observed secular distributions of monthly Paris precipitation (mm.month-1) since 1700. (c) As in (b) for a seasonal reconstructed northern France precipitation index (mm.season-1) since 1500. Grey contours delineate the area above which precipitation is greater than the multi-decadal mean (~60 year smoothing window).
291x298mm (300 x 300 DPI)

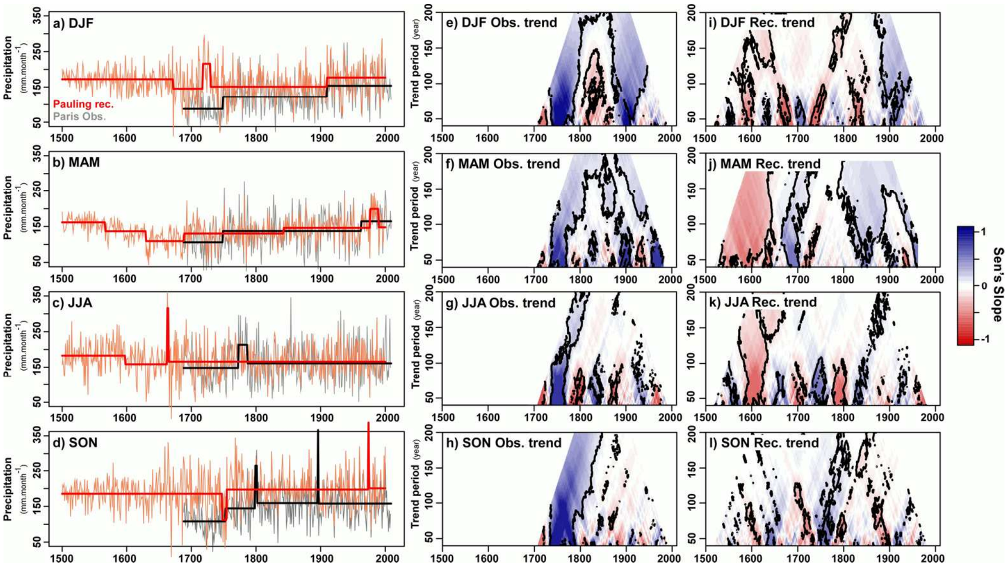

Figure 4. Modifications in mean and trend of seasonal precipitation amounts in northern France over the last five centuries. (a-d) Multiples changes of the means in the observed (grey) and reconstructed (light red) seasonal precipitation time series (mm.season-1; winter: DJF; spring: MAM; summer: JJA; autumn: SON). Bold lines display optimal breaks between adjacent segments with means that are significantly different from the Scheffe contrast test at the 95% confidence interval as determined by a segmentation procedure. (e-h) Two-dimensional diagrams of every possible trend in the observed seasonal precipitation time series as determined by a modified Mann-kendall test. Trend strength (positive: blue; negative: red) is estimate using the Sen's slope while statistical significance at p = 0.05 (contour) is assumed by the two-sided p-values. (i-l) As in (e-h) for a seasonal reconstructed northern France precipitation index (mm.season-1) since 1500.

187x104mm (300 x 300 DPI)

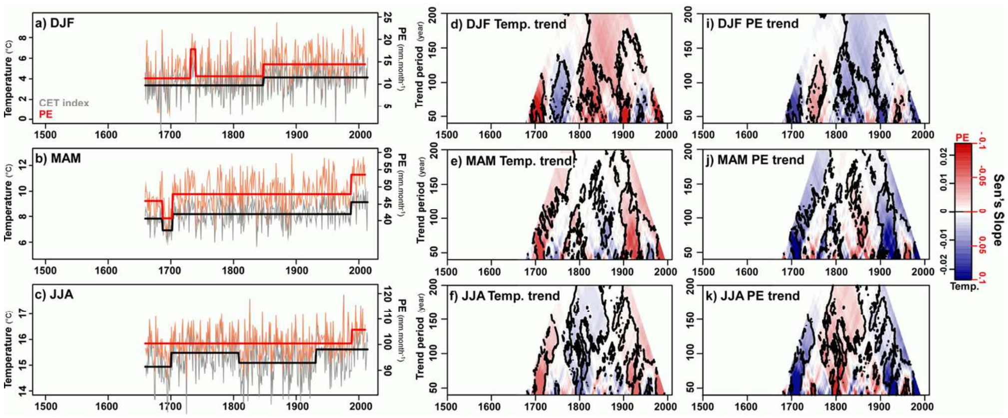

Figure 5. Modifications in mean and trend of seasonal central England temperature and its associated evapotranspiration (PE) over the last centuries. (a-c) Multiples changes of the means in observed temperature (°C; grey) and PE (mm; light red) winter: DJF; spring: MAM; summer: JJA). Bold lines display optimal breaks between adjacent segments with means that are significantly different from the Scheffe contrast test at the 95% confidence interval as determined by a segmentation procedure. (d-f) Two-dimensional diagrams of every possible trend in observed temperature as determined by a modified Mann-kendall test. Trend strength (positive: red; negative: blue) is estimate using the Sen's slope while statistical significance at p = 0.05 (contour) is assumed by the two-sided p-values. (g-k) As in (e-h) for PE (positive: blue; negative: red) since 1500.
137x56mm (300 x 300 DPI)

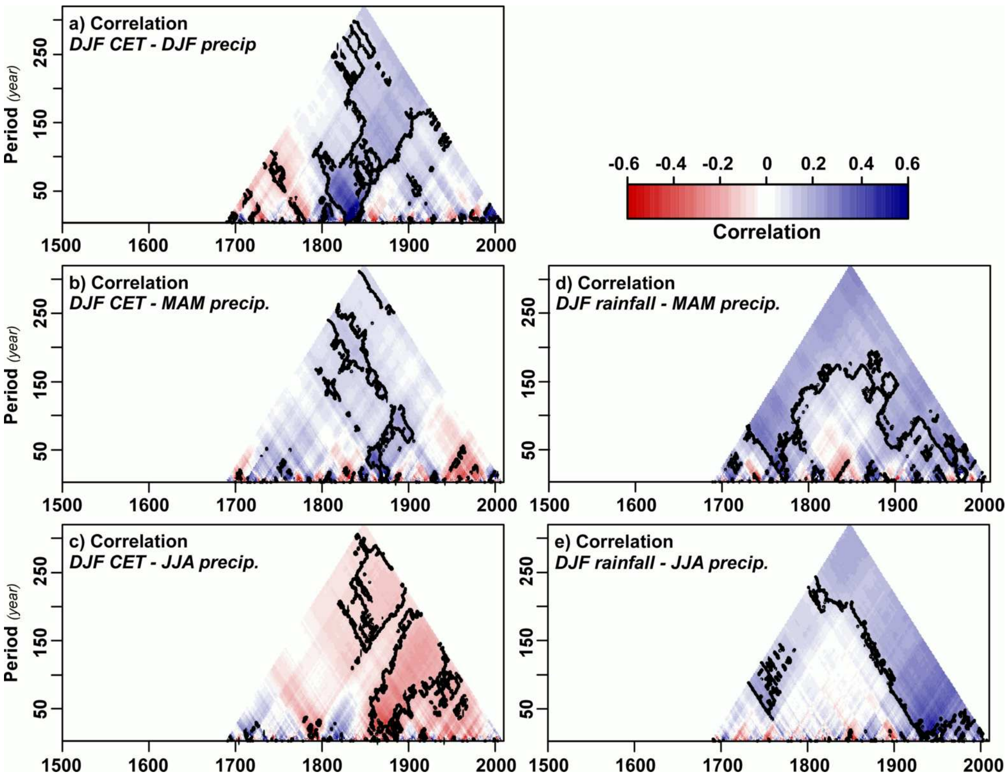


Figure 6. Time-scale evolution of relationships between winter temperature/precipitation and seasonal precipitation average. (a-c) Two-dimensional diagrams of every possible correlation between winter temperature and winter precipitation (at the top), spring precipitation (at the middle) and summer precipitation (at the bottom). (d-e) as for (b-c) but for the correlation between winter precipitation and spring and summer precipitation. Contours indicate correlations statistically significant at p = 0.05 of Pearson's product moment correlation coefficient assuming independent normal distributions. Note that the degrees of freedom (DOF) in the significance calculations are adjusted using the estimated decorrelation scales.
217x166mm (300 x 300 DPI)

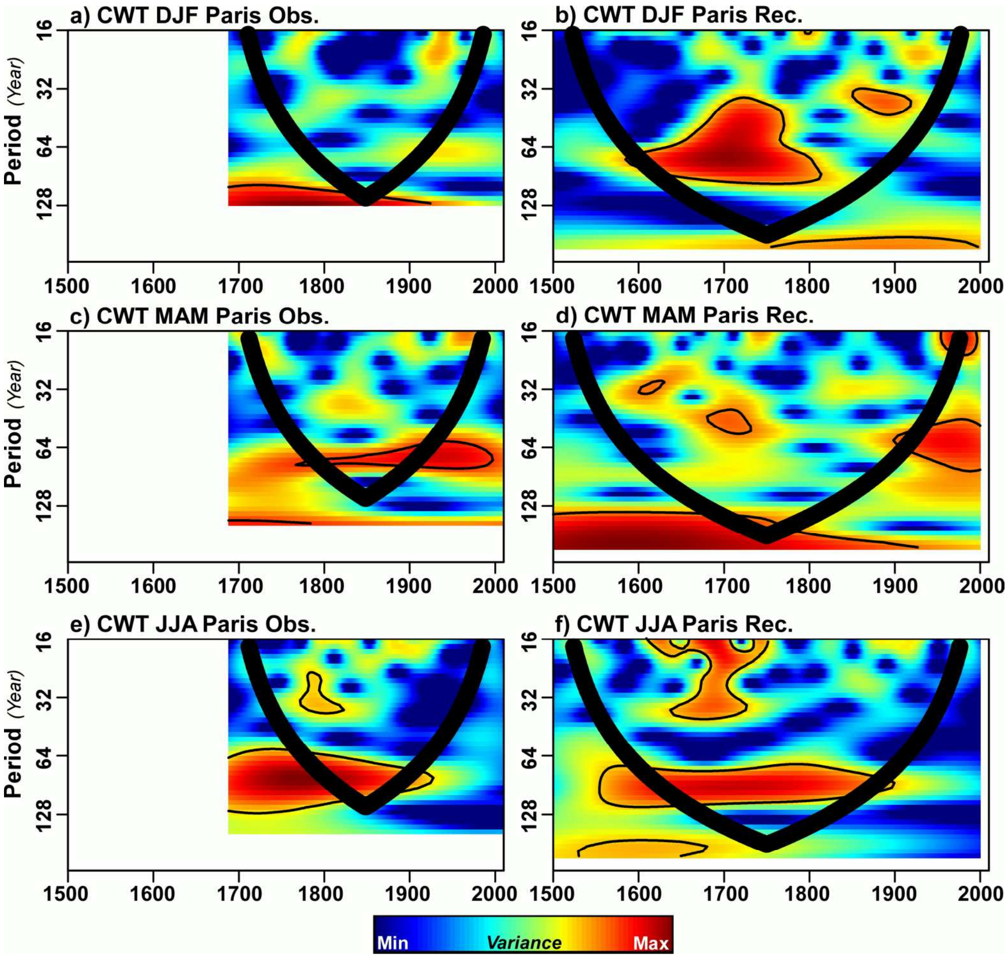


Figure 7. Time-scale patterns of variability in the seasonal precipitation amounts of northern France. (a-f) Wavelet power spectrum of observed (left column) and reconstructed (right column) seasonal precipitation time series (winter: DJF; spring: MAM; summer: JJA). The very thick bold lines (the so-called cone of influence) delineates the area under which power can be underestimated as a consequence of edge effects, wraparound effects and zero padding; thin contour lines show the 95% confidence limits based on 1000 Monte-Carlo simulations of the red noise background spectrum. Note that these time-scale patterns were also obtained without padded with zeroes near the edge of the time series.
269x255mm (300 x 300 DPI)

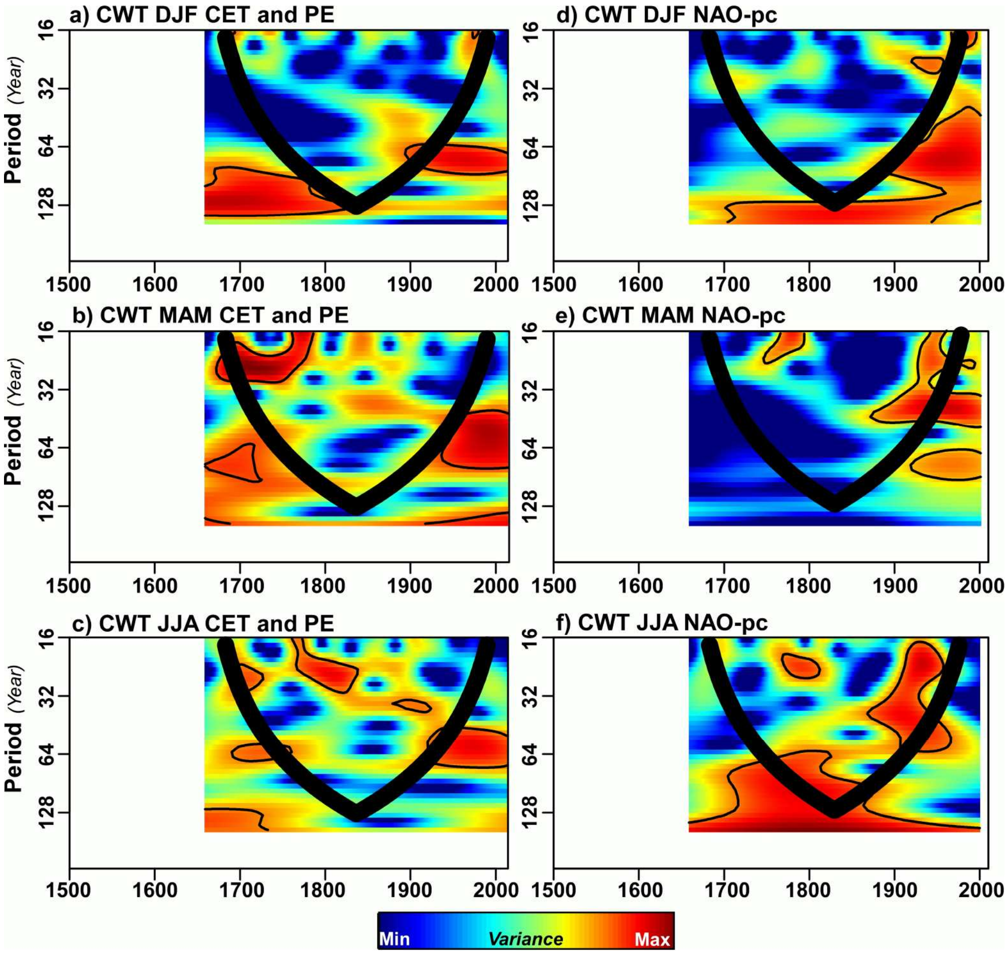


Figure 8. Time-scale patterns of variability in seasonal temperature (and PE) and in the NAO indices. (a-c) Wavelet power spectra of seasonal central England temperature (CET; °C), which are similar to those of PE (winter: DJF; spring: MAM; summer: JJA). (d-f) as in (a-c) for the PC-based seasonal NAO indices. The very thick bold lines (the so-called cone of influence) delineates the area under which power can be underestimated as a consequence of edge effects, wraparound effects and zero padding; thin contour lines show the 95% confidence limits based on 1000 Monte-Carlo simulations of the red noise background spectrum. Note that these time-scale patterns were also obtained without padded with zeroes near the edge of the time series.
268x253mm (300 x 300 DPI)

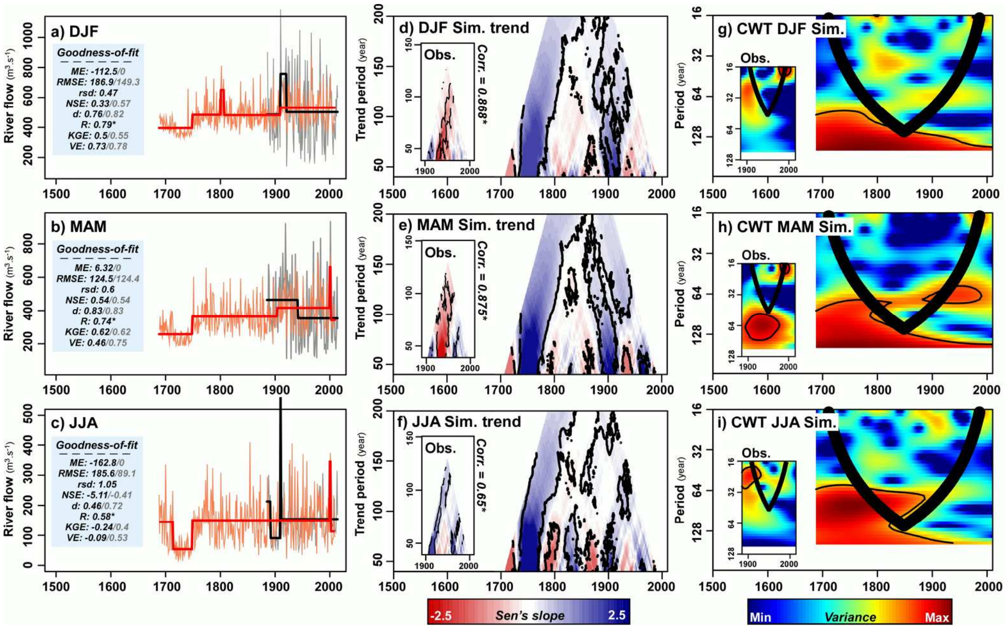

Figure 9. Evaluation of modifications in mean, trend and decadal variability of Paris river flow by GR2M hydrological modelling. (a-c) Multiples changes of the seasonal means (winter: DJF; spring: MAM; summer: JJA) in observed (grey lines) and simulated Paris river flow (red lines; m3.s-1). Bold lines display optimal breaks between adjacent segments with means that are significantly different from the Scheffe contrast test at the 95% confidence interval as determined by a segmentation procedure. The light blue boxes indicate goodness-of-fit measures between observed and simulated values with regard to the common period (1885–2009) before (black) and after (grey) the mean corrections. (d-f) Two-dimensional diagrams of every possible trend in seasonal observed (small box) and simulated river flow as determined by a modified Mann-kendall test. Trend strength (positive: blue; negative: red) is estimate using the Sen's slope while statistical significance at p = 0.05 (contour) is assumed by the two-sided p-values. Correlations between observed and simulated trend patterns, and their statistical significances at p = 0.05, over the common period are indicated on the upper right corners of the observed diagrams. (g-i) Wavelet power spectra of seasonal observed (small box) and simulated river flow. The very thick bold lines (the so-called cone of influence) delineates the area under which power can be underestimated as a consequence of edge effects, wraparound effects and zero padding; thin contour lines show the 95% confidence limits based on 1000 Monte-Carlo simulations of the red noise background spectrum.
214x133mm (300 x 300 DPI)

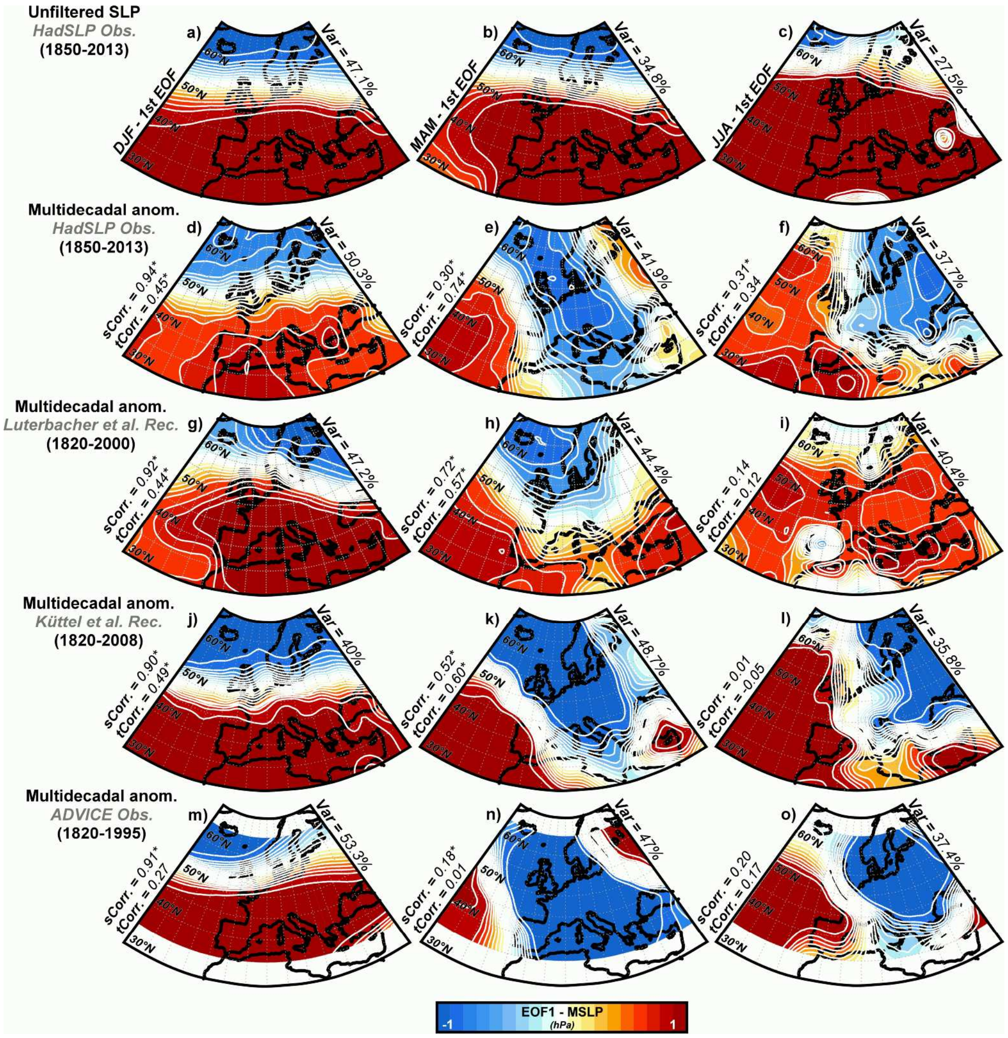


Figure 10. Seasonal NAO patterns and multidecadal anomalies in North Atlantic SLP during the Modern period. (a-c) Seasonal 1st EOF of unfiltered North Atlantic SLP (30° – 70°N; 30°W – 40°E), i.e., NAO patterns, from the HadSLP2r dataset during the modern period. (d-f) Reconstruction using EOF of multidecadal anomalies (i.e., 30-year running mean) in the winter to summer observed North Atlantic SLP during the modern period. (g-l) as for (d-f) but using SLP reconstructions from Luterbacher et al. (2002) and Küttel et al. (2010). (m-o) idem based on ADVICE observation fields. Fraction of the variance expressed by each 1st EOFs are displayed on the upper right corners. Spatial and temporal correlation (sCorr. and tCorr.) between multidecadal anomalies and the NAO (i.e., observed NAO patterns and multidecadal variability extracted from the NAO indices for each dataset) are indicated on the lower left corners. Asterisks indicate significant correlations at p = 0.05 with regard to Dutilleul's and Pearson's t-tests accounting for spatial and temporal autocorrelation.
391x403mm (300 x 300 DPI)

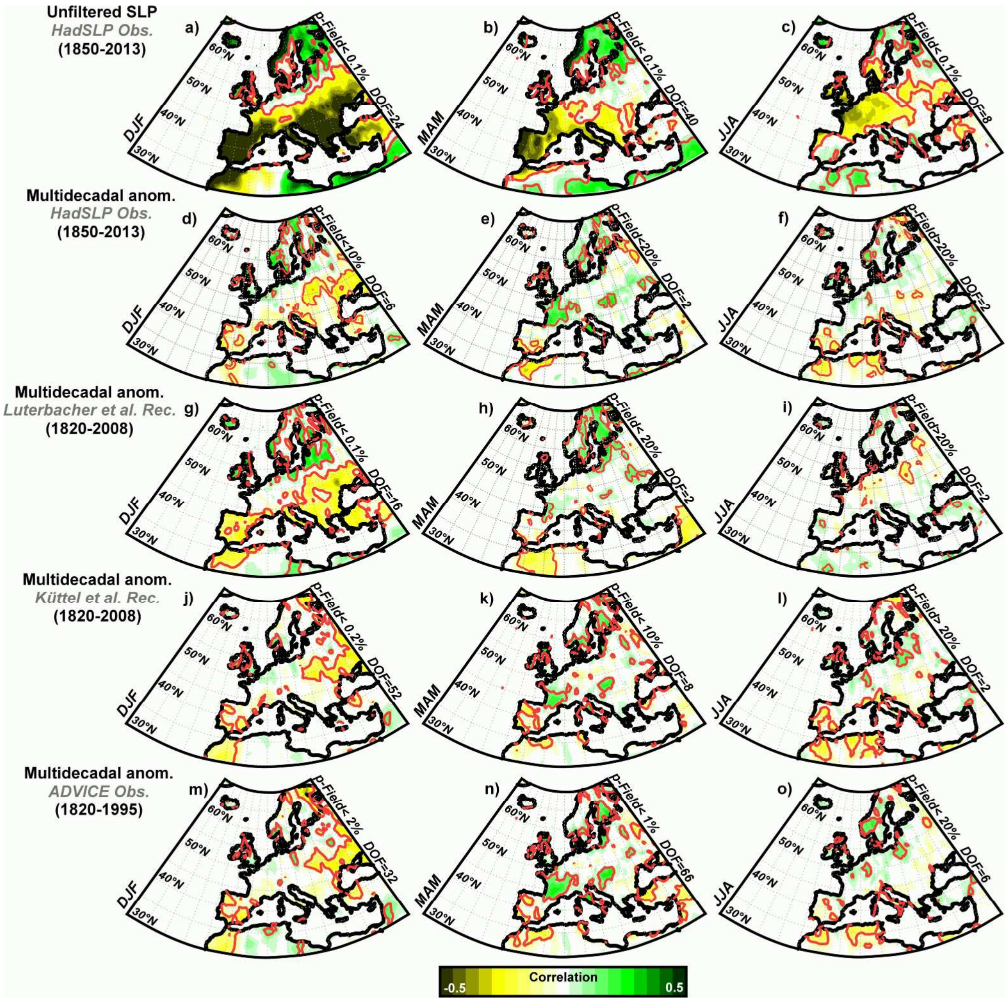


Figure 11. Seasonal correlation patterns between European precipitation and the NAO, as well as the multidecadal North Atlantic SLP anomalies during the Modern period. (a-c) Pointwise correlations between seasonal PC-based NAO indices from HadSLP2r dataset and European precipitation during the Modern period. (d-f) Seasonal pointwise correlations between the 30-year running mean of European precipitation and observed multidecadal North Atlantic SLP anomalies during the Modern period. (g-l) as for (d-f) but using SLP reconstructions from Luterbacher et al. (2002) and Küttel et al. (2010). (m-o) idem based on ADVICE observation fields. Note that the degrees of freedom (DOF) in the significance calculations are adjusted using the estimated decorrelation scales, so the signal may not be more significant after the low-pass filtering. The p-values at the 95% (i.e., p=0.05) confidence level are computed against a 1000 sample Monte-Carlo simulations, where the precipitation fields are replaced with red noise. Field significance and the spatial DOF are displayed on the upper right corners.
390x388mm (300 x 300 DPI)